

# Rain-on-snow responses to a warmer Pyrenees: a sensitivity analysis using a physically-based hydrological model

Josep Bonsoms<sup>1</sup>, Juan I. López-Moreno<sup>2</sup>, Esteban Alonso-González<sup>3</sup>, César Deschamps-Berger<sup>2</sup>, Marc Oliva<sup>1</sup>

<sup>1</sup> Department of Geography, Universitat de Barcelona, Barcelona, Spain

<sup>2</sup> Instituto Pirenaico de Ecología (IPE-CSIC), Campus de Aula Dei, Zaragoza, Spain

<sup>3</sup> Centre d'Etudes Spatiales de la Biosphère (CESBIO), Université de Toulouse, CNES/CNRS/IRD/UPS, Toulouse, France.

Corresponding author: Juan I. López-Moreno (nlopez@ipe.csic.es)

**Abstract.** Climate warming is changing the magnitude, timing, and spatial patterns of mountain snowpacks. A warmer atmosphere may also ~~induce~~~~lead to~~ precipitation phase shifts, ~~with resulting in a~~ decreased snowfall fraction (Sf). The combination of Sf and snowpack ~~decreases~~ directly ~~influences~~~~affects~~ the frequency and intensity of rain-on-snow (ROS) events, a common cause of flash-flood events in snow-dominated regions. In this work, we ~~investigate~~~~examine the~~ ROS patterns and ~~their~~ sensitivity to temperature and precipitation changes in the Pyrenees ~~by~~ modelling ROS through a physically-based snow model. ~~This model is~~ forced with reanalysis climate data ~~for elevations of 1500 m, 1800 m, and 2400 m~~ perturbed using a range of ~~values~~ ~~of~~-temperature and precipitation ~~values~~ consistent with 21<sup>st</sup>-century climate projections. ROS patterns are characterized by their frequency, rainfall quantity, and snow ablation. The highest ROS frequency for the historical climate period (1980 – 2019) ~~is~~~~are~~ found in ~~the 2400 m zones of the~~ South-West ~~high elevations~~ ~~sectors of the~~ Pyrenees (17 days/year). ~~The~~ ~~M~~maximum ROS rainfall amount is detected in ~~1800 m areas of~~ ~~the~~ South-East ~~mid elevations areas~~ (45 mm/day, autumn), whereas the highest ROS ablation is found in ~~the~~ ~~2400 m zones of the~~ North-West ~~high elevations zones~~ ~~(- 10 cm/day, summer)~~. When air temperature ~~increases~~~~is increased~~ from 1°C to 4°C ~~with respect~~~~compared~~ to the historical climate period, ROS rainfall amount and frequency increase at a constant rate during winter and early spring for all elevation zones. For the rest of the seasons, non-linear responses of ~~the~~ ROS frequency and ablation to warming are found. Overall, ROS frequency decreases in the shoulders of the season across ~~eastern~~~~Eastern~~ low-elevated zones due to snow cover depletion. However, ROS increases in cold, high-elevated zones where long-lasting snow cover exists until late spring. Similarly, warming induces greater ~~ROS~~ ablation (+ 10% per °C) during the coldest months of the season, ~~high~~~~2400 m~~ elevations, and northern sectors, where the deepest snow depths are found. On the contrary, small differences in ROS ablation are found for warm and marginal snowpacks. These results highlight the different ROS responses to warming across the mountain range, suggest similar ROS sensitivities in near mid-latitude zones, and will help anticipate future ROS impacts in hydrological, environmental, and socioeconomic mountain systems.

**Keywords:** Snow, Rain-on-snow, Climate warming, Snow sensitivity, Mountain snowpack, Pyrenees.

## 1 Introduction

Mountain snowpacks supply large hydrological resources to the lowlands (García-Ruiz et al., 2015; Viviroli et al., 2011; Immerzeel et al., 2020), with important implications ~~for in the~~ ecological (Wipf and Rixen, 2010), ~~hydrological (Barnett, 2005; Immerzeel et al., 2020)~~ and socioeconomic systems, ~~by~~ providing hydroelectricity (Beniston et al., 2018) ~~and supporting or guaranteeing~~ winter tourism activities (Spandre et al., 2019). ~~However, Climate warming, however, is~~ ~~modifying altering~~ mountain snowfall patterns (Hock et al., 2019) ~~(IPCC, 2022), through temperature induced precipitation changes from snowfall to rainfall by~~ ~~decreasing the snowfall fraction (Sf)~~ (Lynn et al., 2020), leading in some cases to rain-on-snow (ROS) events in snow-covered areas, where ~~they~~ ~~it~~ did not occur ~~(often)~~ before. The upward ~~high-latitude~~ temperature ~~and precipitation~~ trends (Bintanja and Andry, 2017) ~~and warming~~ in mountain regions (Pepin et al., 2022) ~~are will~~ likely ~~to~~ change future ROS frequency in snow-dominated areas (López-Moreno et al., 2021).

ROS has relevant impacts ~~on the mountain ecosystem dynamics (Hock et al., 2019).~~—The liquid water percolation in the snowpack due to a ROS event creates ice layers and could alter its stability (Rennert et al., 2009). In severe ROS events, water percolation reaches the ground, and the subsequent water freezing causes latent heat releases, leading to soil ~~(and permafrost)~~ warming (Westermann et al., 2011). Positive heat fluxes during ROS events enhance snow runoff (Corripio and López-Moreno, 2017), especially in warm and wet snowpacks (Würzer et al., 2016). ROS can also ~~induce trigger~~ a snow avalanches in mountain zones (Conway and Raymond, 1993), ~~contribute to~~ flash flood events (Surfleet and Tullos, 2013), ~~affect impacts in~~ tundra ecosystems (Hansen et al., 2014) and ~~impact~~ herbivore populations (Kohler and Aanes, 2004).

Different ROS frequency trends have been found since the last half of the 20<sup>st</sup> century. In the ~~western~~ ~~United States~~ ~~United States~~, ~~and~~ from 1949 to 2003, (McCabe et al., 2007) found a general ROS frequency decrease ~~at~~ 1500 m but an increase in high elevations. Similarly, the analysis of six major German basins from 1990 to 2011, ~~reveals~~ ~~a~~ ~~n upward (downward)~~ ROS frequency trend during ~~winter (spring)~~ at ~~1500~~ ~~low~~ and high elevations (Freudiger et al., 2014). On the contrary, from 1979 to 2014, no winter ROS frequency trends were found across the entire Northern ~~Hemisphere~~ (Cohen et al., 2015). ROS projections for the end of the 21<sup>st</sup> century suggest a general ROS frequency increase in cold regions and high elevated zones (Hock et al., 2019) ~~IPCC, 2019~~. This is projected for Alaska (Bieniek et al., 2018), Norway (Mooney and Li, 2021), ~~the western~~ ~~Western~~ ~~United States~~ ~~United States~~ (Musselman et al., 2018), Canada (il Jeong and Sushama, 2018) or Japan (Ohba and Kawase, 2020). In European mid-latitude mountain ranges, such as the Alps, ROS frequency is expected to increase ~~at high-elevation~~ ~~sectors~~ ~~areas~~ ~~but decrease at low-elevation~~ ~~sectors (decrease) in high (low) elevation sectors~~ (Beniston and Stoffel, 2016; Morán-Tejeda et al., 2016). López-Moreno et al. (2021) compared the ROS sensitivity to climate warming across 40 global basins and detected the highest ROS frequency decreases in low-elevated and warm Mediterranean mountain sites.

64 Despite the increasing understanding of ROS spatio-temporal past and future trends, little is known about the  
65 ROS sensitivity to climate warming across southern European mountain ranges, such as the Pyrenees.

66  
67 Here, we examine the ROS sensitivity to temperature and precipitation changes for low (1500 m), mid (1800  
68 m), and high (2400 m) elevations of the Pyrenees. ROS responses to temperature and precipitation ~~are~~  
69 analyzed using a physically-based snow model, forced with reanalysis climate data (1980 – 2019 ~~period~~)  
70 perturbed according to a range of temperature and precipitation changes consistent with 21<sup>st</sup> century climate  
71 projections for the mountain range (Amblar-Francés et al., 2020). Previous studies in alpine zones have shown  
72 different ROS responses to warming depending on the area and month of the season (e.g., Morán-Tejeda et al.  
73 2016). For this reason, results are focused on these two factors. First, we analyze height of snow (HS) and  
74 snowfall fraction (Sf) responses to temperature and precipitation since these are the main variables that control  
75 ROS events (López-Moreno et al., 2021). Next, we examine ROS patterns and their response to warming  
76 ~~using~~ three key ROS indicators, namely:

- 77  
78 (a) Number of ROS days for a season (ROS frequency).  
79 (b) Average rainfall quantity during a ROS day (ROS rainfall amount).  
80 (c) Average daily snow ablation during a ROS day (ROS ablation).

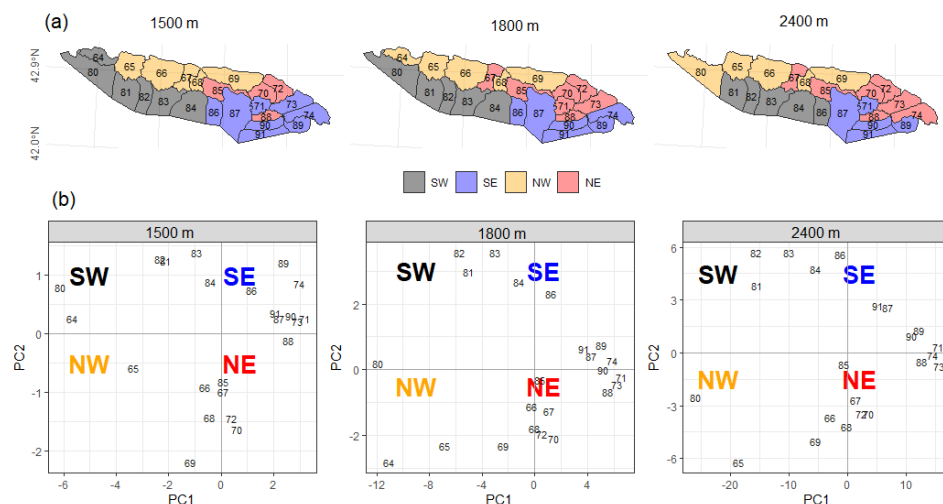
81  
82 The study area is presented in Section 2. Section 3 describes the data and methods. Section 4 presents the  
83 results. ~~Finally, We finally in Section 5 we~~ discuss the anticipated ROS spatio-temporal changes, their socio-  
84 environmental impacts, and hazards. ~~in Section 5.~~

## 85 86 2 Regional setting

87  
88 The Pyrenees ~~Mountain-mountain~~ range is located between the Atlantic Ocean (West) and the Mediterranean  
89 Sea (East), and ~~is-constitutes~~ the largest (~ 450 km) mountain range of the Iberian Peninsula. Elevation  
90 increases towards the central massifs, where the highest peaks ~~is-are~~ found (e.g. Aneto, 3,404 m asl). Glaciers  
91 expanded during the Little Ice Age and nowadays are ~~only found~~ the highest mountain summits (Vidaller  
92 et al., 2021). The regional annual 0 °C isotherm ~~is-lies~~ at ~~approximately~~ 2700 m (Del Barrio et al., 1990),  
93 and at ~~about~~ 1600 m during the cold season (López-Moreno and Vicente-Serrano, 2011). The elevation  
94 lapse-rate is ~~approximately~~ 0.56°/100 m, being slightly lower during winter (Navarro-Serrano and  
95 López-Moreno, 2017). ~~Average~~ annual precipitation is ~~approximately~~ 1000 mm/year ~~at 1000 m (Bonsoms~~  
96 ~~et al., 2023a).~~ ~~(ca. 1500 m);~~ ~~m~~ Maximum values are found in the ~~Northern-Western (NW)~~ ~~northern-western~~  
97 massifs, ~~(around 2000 mm/year)~~, decreasing towards the ~~Southern-Eastern (SE)~~ ~~(SE)~~ area (Lemus-Canovas  
98 et al., 2019). Precipitation is predominantly (> 90%) solid above 1600 m from November to May (López-  
99 Moreno, 2005). Due to the mountain alignment, relief configuration, and the distance to the Atlantic Ocean,  
100 seasonal snow accumulations ~~in~~ the northern slopes (~~approximately~~ 500 cm/season), almost doubles ~~those~~  
101 recorded in the SE area ~~for-at~~ the same elevations (~~roughly~~ 2000 m) (Bonsoms et al., 2021~~a~~~~b~~). In the

Western and Central area of the Southern slopes of the range (SW sector, Figure 1), snow accumulation is ruled-influenced by Atlantic wet and mild flows, which are linked with negative North Atlantic Oscillation (NAO) phases (SW and W synoptic weather types) (López-Moreno, 2005; Alonso-González et al., 2020b; Bonsoms et al., 2021a). Positive Western Mediterranean Oscillation (WeMO) phases (NW and NE synoptic weather types) control the snow patterns in the Northern-Eastern (NE) slopes of the range (Bonsoms et al., 2021a). Generally, snow ablation starts in February at low elevations and in May at high elevation. The energy available for snow ablation during spring is controlled by net radiation (55 %, over the total), latent (32 %) and sensible (13 %) while turbulent heat flux increases toward the SE zones of the mountain range heat fluxes (Bonsoms et al., 2022).

111  
112  
113



114

**Figure 1.** (a) Pyrenean massifs sectors (colors) for 1500 m, 1800 m and 2400 m elevation. Massifs were classified-categorized according to through a Principal Component Analysis (PCA) applied to over monthly height of snow (HS) data for each massif and elevation range, considering for all months and years of the historical climate period (1980 – 2019). Panel (b) shows PCA scores for each massif at 1500-m, 1800-m, and 2400 m elevation. The black numbers represent the SAFRAN massif's identity numbers as defined by Vernay et al. (2022). Note that the 2400 m elevation range does not include massif number 64, as this massif does not reach that elevation range.

121  
122

### 123 3 Data and methods

124

#### 125 3.1 Snow model description

126

127 The snowpack is simulated using the energy and mass balance snow model FSM2 (Essery, 2015). The FSM2  
 128 was forced at an hourly resolution for each massif and elevation range (c.f. Sect. 3.3) ~~during for~~ the historical  
 129 climate period (1980 – 2019) and perturbed using a range of values of temperature and precipitation changes  
 130 consistent with 21<sup>st</sup> century climate projections (c.f. Sect. 3.4). Sf was quantified using a threshold-approach.  
 131 Precipitation was ~~considered as~~ snowfall when ~~the~~ temperature was  $< 1\text{ }^{\circ}\text{C}$ , ~~in accordance with~~ according to  
 132 previous ROS research in the study zone (Corripio and López-Moreno, 2017), and the average rain-snow  
 133 temperature threshold for the Pyrenees (Jennings et al., 2018). Snow cover fraction is calculated by a linear  
 134 function of snow depth, and snow albedo is estimated based on a prognostic function with the new snowfall.  
 135 Snow thermal conductivity is estimated based on snow density, and, ~~L~~liquid water percolation is calculated  
 136 based on a gravitational drainage. ~~The c~~Compaction rate is simulated from overburden and thermal  
 137 metamorphism. ~~The a~~Atmospheric stability is estimated through ~~the~~Richardson number stability functions to  
 138 simulate latent and sensible heat fluxes. The selected FSM2 configuration includes three snow layers and four  
 139 soil layers. The ~~FSM2 configuration selected is shown in Table S1~~ full details of the FSM2 configuration used  
 140 in the present study are shown in Table S1. ~~The This~~ FSM2 model and configuration ~~were as~~ previously  
 141 validated in the Pyrenees ~~by at~~ Bonsoms et al. (2023b). FSM2 has been successfully used in snow model  
 142 sensitivity studies in alpine zones (Günther et al., 2019). ~~FSM2 has been and~~ implemented in a ~~wide range~~  
 143 variety of alpine conditions, ~~such as for the including the mountains of the~~ Iberian Peninsula ~~mountains~~  
 144 (Alonso-González et al., 2019), Spanish Sierra Nevada (Collados-Lara et al., 2020) and or ~~Swiss~~ forest  
 145 environments (Mazzotti et al., 2020). ~~snowpack modeling~~. The FMS2 has also been integrated in snow data-  
 146 assimilation schemes in combination with ~~in situ (Smyth et al., 2022) and~~ remote-sensing data (Alonso-  
 147 González et al., 2022).

148

### 149 3.2 Atmospheric forcing data

150

151 The FSM2 was forced with the SAFRAN meteorological system reanalysis dataset for flat terrain (Vernay et  
 152 al., 2022). The SAFRAN meteorological system integrates meteorological simulations, remote-sensing cloud  
 153 cover data, and instrumental records through data-assimilation. SAFRAN is forced with a combination of  
 154 ERA-40 reanalysis (1958 to 2002) and the numerical weather prediction model ARPEGE (2002 to 2020). The  
 155 SAFRAN system was ~~originally firstly~~ designed for hazard forecasting (Durand et al., 1999, 2009). ~~SS~~SAFRAN  
 156 has been extensively validated as meteorological forcing data for ~~the~~ snow modeling in complex alpine terrain  
 157 (Revuelto et al., 2018; Deschamps-Berger et al., 2022), to studying long-term snow evolution (Réveillet et al.,  
 158 2022), avalanche hazard forecasting (Morin et al., 2020), snow climate projections (Verfaillie et al., 2018),  
 159 snow depth (López-Moreno et al., 2020) and spatiotemporal trends in energy heat fluxes ~~energy heat fluxes~~  
 160 ~~spatio-temporal trends~~ (Bonsoms et al., 2022).

161

### 162 3.3 Spatial areas

163

164 The SAFRAN system provides data at an hourly resolution from 0 to 3600 m, in intervals of ~~by steps of~~ 300

m, grouped by massifs. The SAFRAN massifs (polygons ~~in~~ Figure 1) were ~~selected~~~~chosen~~ for their relative topographical and climatological similarities (Durand et al., 1999). We ~~chose~~ SAFRAN specific elevation bands of ~~selected the~~ 1500 m (low), 1800 m (mid), and 2400 m (high). ~~specific elevation bands of the Pyrenees.~~ ~~In order to retain~~To preserve the main spatial differences across the mountain range, reduce data dimensionality, and ~~capture~~ ~~include the the~~ maximum variance, massifs with similar interannual snow characteristics were grouped into sectors ~~by performing~~ ~~using~~ Principal Component Analysis (PCA). PCA is ~~an extensively~~ ~~a~~ widely applied statistical method for climatological and snow spatial regionalization (~~i.e., e.g.,~~ López-Moreno and Vicente-Serrano, 2007; Schöner et al., 2019; Alonso-González et al., 2020a; Matiu et al., 2021; Bonsoms et al., 2022). A PCA was applied ~~to over~~ HS data for all months and years of the historical climate period. Massifs were ~~categorized~~~~grouped~~ into four groups ~~depending~~ ~~based~~ on the maximum correlation to the first (PC1) and second (PC2) scores. Pyrenean sectors were named South-West (SW), South-East (SE), North-West (NW) and North-East (NE) ~~according~~ ~~due~~ to their geographical position. Figure 1 ~~displays~~~~shows~~ the resulting Pyrenean regionalization for ~~elevations of~~ 1500 m, 1800 m, and 2400 m. ~~elevation~~ as well as the SAFRAN massifs. ~~PC1 and PC2.~~

179

### 180 3.4 Sensitivity analysis

181

ROS season extension was ~~determined~~~~fixed according to~~ ~~based on~~ ROS occurrences during the historical climate period. For the purposes of this research, seasons are ~~categorized~~~~classified~~ as follows: October and November (Autumn); December, January, and February (Winter); March, April, May, and June (Spring); and July (Summer). August and September are ~~not included~~~~excluded~~ due to the absence of regular snow cover. Sf, HS and ROS sensitivity to air temperature and precipitation ~~are~~ ~~is~~ analyzed by perturbing climate data (López-Moreno et al., 2013; Pomeroy et al., 2015; Marty et al., 2017; Musselman et al., 2017b; Rasouli et al., 2019; Alonso-González et al., 2020a; López-Moreno et al., 2021). Specifically, SAFRAN reanalysis climate data was perturbed according to Spanish Meteorological Agency air temperature and precipitation projections for the 21<sup>st</sup> century in the Pyrenees (Amblar-Francés et al., 2020). Precipitation was increased (+10%), left unchanged (0 %) and decreased (- 10%). Air temperature (°C) was perturbed between +1°C and +4°C ~~in~~ ~~by~~ steps of ~~±~~ 1°C. Incoming longwave radiation ~~was~~ increased due to warming, by applying the Stefan-Boltzmann law, using the Stefan-Boltzmann constant ( $\sigma$ ;  $5.670373 \times 10^{-8} \text{ W m}^{-2} \text{ K}^{-4}$ ), and the hourly atmospheric emissivity ( $\epsilon_t$ ) derived from SAFRAN air temperature and incoming longwave radiation:

195

196

197

$$\epsilon_t = \frac{LW_{in}}{\sigma(T_a + 273.15)^4}$$

Where  $T_a$  is air temperature and  $LW_{in}$  is incoming longwave radiation. An increase ~~in~~ ~~of~~ air temperature of 1°C can be interpreted as a low-emission scenario for the region, while 2°C and 4°C would represent projections for mid and high-emission scenarios, respectively (Pons et al., 2015). The range of +/-10% for precipitation includes the expected changes in precipitation according to most climate models, ~~irrespective~~~~regardless~~ of the

202 emission scenario (López-Moreno et al., 2008; Pons et al., 2015; Amblar-Francés et al., 2020).

203

### 204 3.5 ROS definition and indicators

205

206 The average ~~HS and Sf~~ sensitivity of HS and Sf to temperature and precipitation (expressed ~~as~~ % per °C of  
207 local warming) is calculated as the average seasonal HS and Sf anomalies compared to the historical  
208 climate period, ~~and~~ divided by degree of warming. ROS dDays are classified ~~as ROS days~~ when the daily  
209 rainfall amount ~~is~~  $\geq 10$  mm and HS  $\geq 0.1$  m, ~~according to previous works~~ (Musselman et al., 2018;  
210 López-Moreno et al., 2021). ROS frequency corresponds to the number of ROS days. ROS rainfall amount  
211 (mm/day) ~~represents~~ the average daily rainfall (mm) during a ROS day. ROS ablation is the average daily  
212 snow ablation (cm/day) during a ROS day. The average daily snow ablation is determined by the daily average  
213 HS difference between two consecutive days (Musselman et al., 2017a). Only the days when a negative HS  
214 difference occurred were selected.

215

## 216 4 Results

217

218 We ~~present~~ provide an analysis of Sf, HS, and ROS patterns in response to temperature and precipitation  
219 changes. The spatiotemporal dynamics of ROS ~~spatio-temporal dynamics are analyzed-examined~~ in terms of  
220 frequency, rainfall quantity and snow ablation. ~~Since we have detected a non-linear~~ Given the identified non-  
221 linear sensitivity of ROS ~~sensitivity~~ to temperature, the values of ROS indicators ~~values are shown~~ are displayed  
222 as a function of ~~the~~ changes in temperature and precipitation amounts, grouped-categorized by elevation and  
223 sectors, namely SW, SE, NW and NE.

224

### 225 4.1 HS and Sf response to temperature and precipitation changes

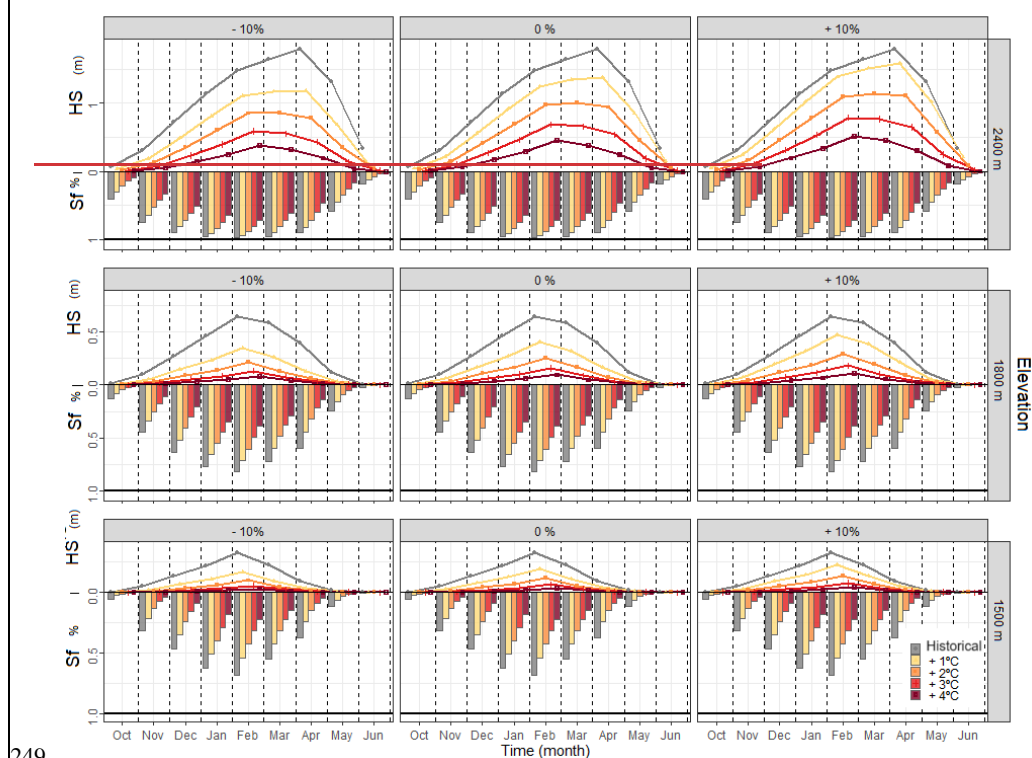
226

227 Figure 2 show the HS and Sf-response of HS and Sf to temperature and precipitation, ~~is shown in Figure 2.~~  
228 The seasonal variability of HS and Sf ~~variability is primarily influenced mostly controlled by the increment~~  
229 ~~of~~ by temperature, season, elevation, and spatial sectors. As shown in Figures 2, S1, S2 and S3, precipitation  
230 variability plays a moderate to low role in seasonal HS evolution. ~~The role of precipitation variability in the~~  
231 ~~seasonal HS evolution is moderate to low (Figure S1 to S3). Only at an elevation of 2400 m, elevation an~~  
232 ~~upward trend of in precipitation (at least > 10%) can counterbalance small temperature increments increments~~  
233 ~~of temperature (< 1°C), over the historical climate period), from December to February (Figure S34). For this~~  
234 ~~reason, Consequently,~~ precipitation was excluded ~~from~~ further analysis, ~~and the ROS sensitivity analysis is~~  
235 ~~evaluated for the average change of precipitation.~~ While S snow at 1500 m and 1800 m elevations ~~during~~  
236 ~~summer~~ is rarely simulated observed during summer, ~~however,~~ marginal snow cover at 2400 m elevation can  
237 ~~persist~~ last until June and July, ~~especially particularly~~ in the wettest sectors of the range (NW and SW). The  
238 response of S seasonal HS and Sf ~~response to~~ temperature ~~show-exhibits~~ large seasonality. The average HS  
239 reduction ~~ranges from~~ 39 %, 37 % and 28 % per °C, for 1500 ~~m-m~~, 1800 ~~m-m~~ and 2400 m elevations,

240 respectively. However, ~~important~~<sup>relevant</sup> differences are found depending on the season and degree of  
 241 warming (Figures 2 and 3). Maximum HS and Sf reductions ~~are found in~~<sup>occur at</sup> 1500 m and 1800 m  
 242 elevations during the shoulders of the season (autumn and spring). ~~At~~<sup>in</sup> these elevations, ~~the~~<sup>the</sup> maximum HS  
 243 decreases (52 % over the historical climate period) are simulated for spring when ~~the~~<sup>the</sup> temperature is ~~+~~<sup>increased</sup>  
 244 1°C. The greatest HS decreases in ~~areas at~~<sup>at</sup> 2400 m elevation ~~areas~~<sup>are</sup> are simulated for summer (54 % HS decrease  
 245 for 1°C). If temperature reaches maximum values (+ 4 °C), seasonal HS is reduced by 92 %, 89 %, and 79 %  
 246 for ~~elevations of~~<sup>elevations</sup> 1500 m, 1800 m, and 2400 m ~~elevations~~<sup>respectively</sup> (Figure S4).

247

248



249



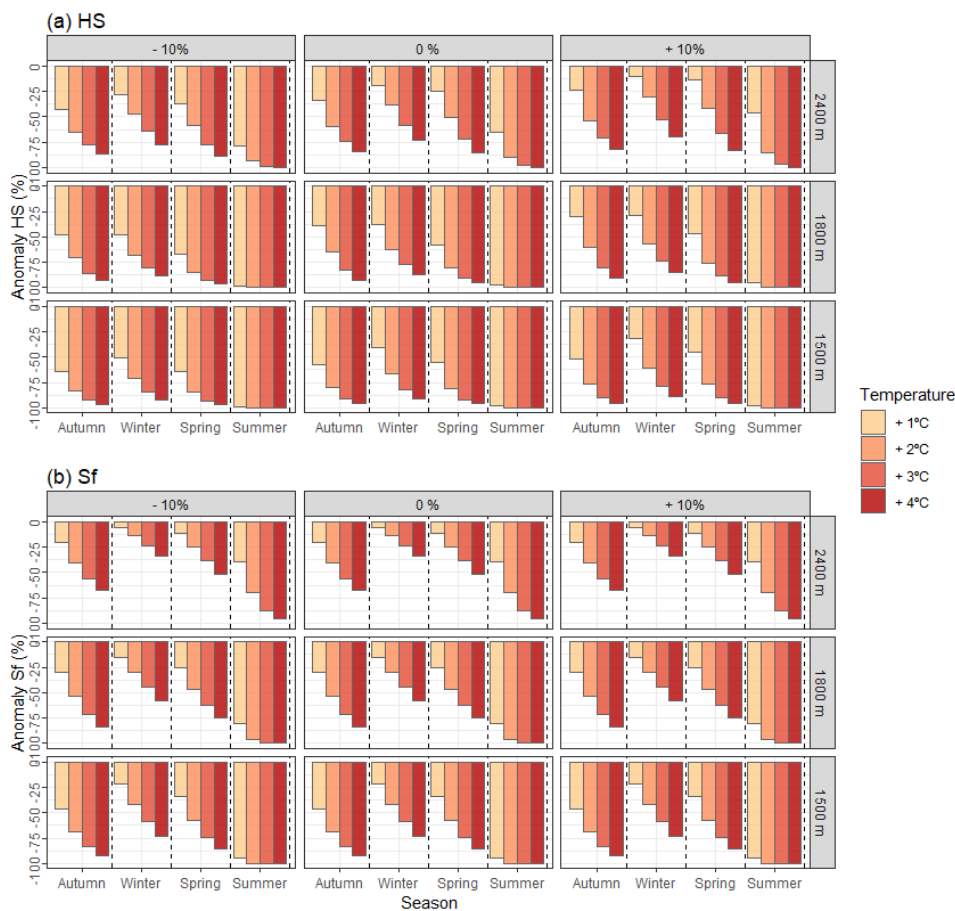


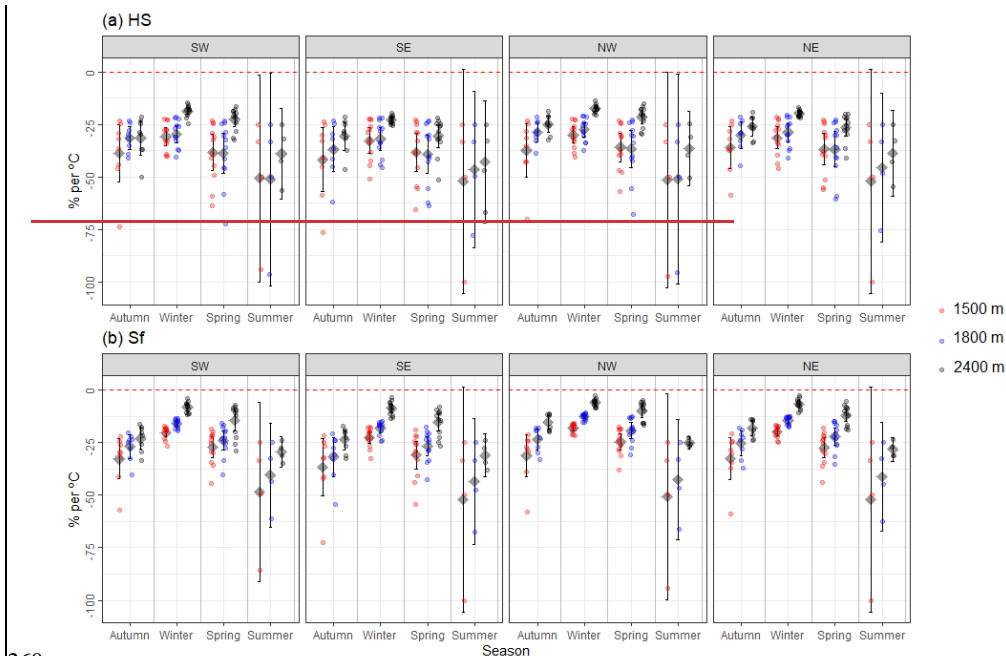
**Figure 2.** Seasonal (a) height of snow (HS) and (b) snowfall fraction (Sf) anomalies with respect to the historical climate period (1980 – 2019). Data are shown by different increments of temperature (colors) grouped by precipitation changes and elevations (boxes). **Figure 2.** Height of snow (HS) (lines) and Snowfall fraction (Sf) (bars) monthly variation for the historical climate period (1980 – 2019) and different increments of temperature (colors) grouped by precipitation change and elevation (boxes). Note that Sf values (y axis) are inverted.

**Con formato:** Fuente: Sin Negrita

**Con formato:** Interlineado: 1,5 líneas

**Con formato:** Fuente: Sin Negrita

**Con formato:** Fuente: Sin Negrita



260  
 261  
 262 **Figure 3.** Seasonal (a) HS and (b) Sf anomalies over the historical climate period (1980–2019). Data are  
 263 shown by elevation (colors), season (x axis) and sectors (boxes). Points represent the average seasonal HS  
 264 and Sf anomalies grouped by month of the season and increment of temperature (from 1°C to 4°C). The black  
 265 diamond point indicates the mean, whereas the upper and lower error bars show the Gaussian confidence  
 266 based on the normal distribution. Data are the average of the simulated precipitation change (from -10% to  
 267 +10%, by steps of 10%).  
 268  
 269 Sf shows lower sensitivity to warming than HS, with and maximum reductions in autumn. On average, Sf  
 270 decreases by 29 %, 22 %, and 12 % per °C for elevations of 1500 m, 1800 m, and 2400 m elevations,  
 271 respectively. An increase of 4°C leads to Sf reductions of 80 %, 69 % and 49 % for elevations of 1500 m, 1800  
 272 m, and 2400 m elevations. Independently-Regardless of the elevation band and season, the SE sector exhibit  
 273 the greatest HS and Sf decreases (41 % and 35 % per °C, respectively). On the contrary, minimum reductions  
 274 are expected on the northern slopes (NW and NE).

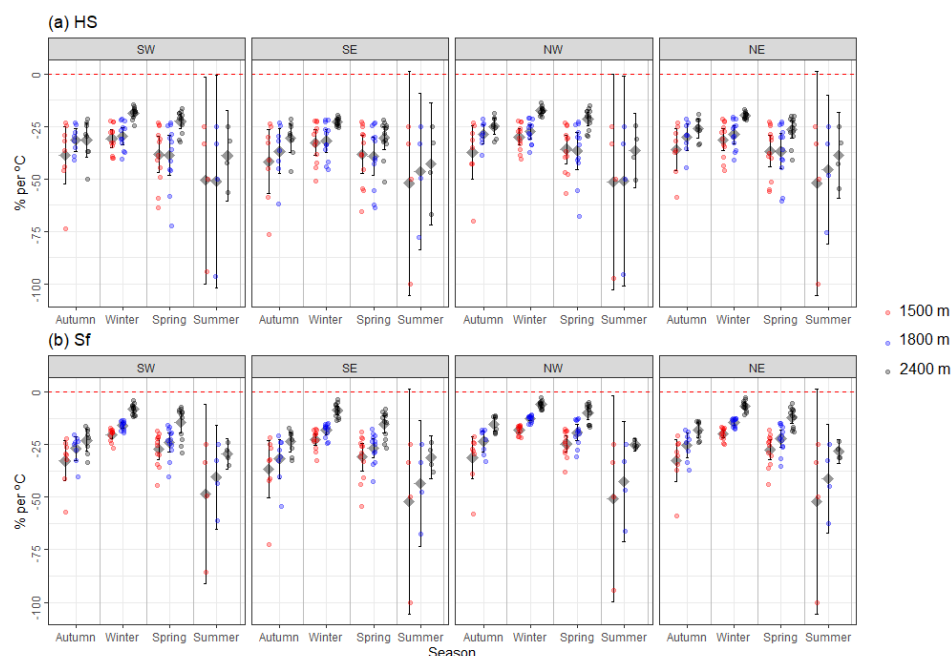


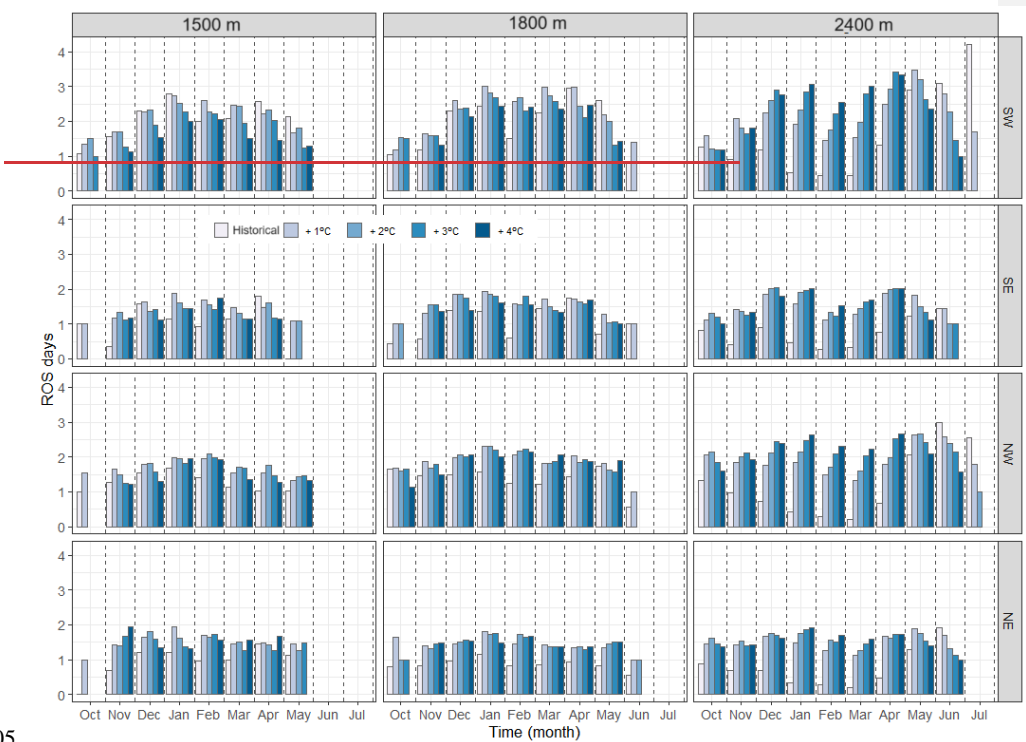
**Figure 3.** Seasonal (a) height of snow (HS) and (b) snowfall fraction (Sf) anomalies over the historical climate period (1980 – 2019). Data are shown by elevation (colors), season (x-axis), and sectors (boxes). Points represent the average seasonal HS and Sf anomalies grouped by the month of the season and increment of temperature (from 1°C to 4°C, with increments of 1°C). The black diamond point indicates the mean, whereas the upper and lower error bars show the Gaussian confidence based on the normal distribution. Data represent the average of the simulated precipitation change (from - 10% to 10%, with increments of 10%).

## 4.2 ROS frequency

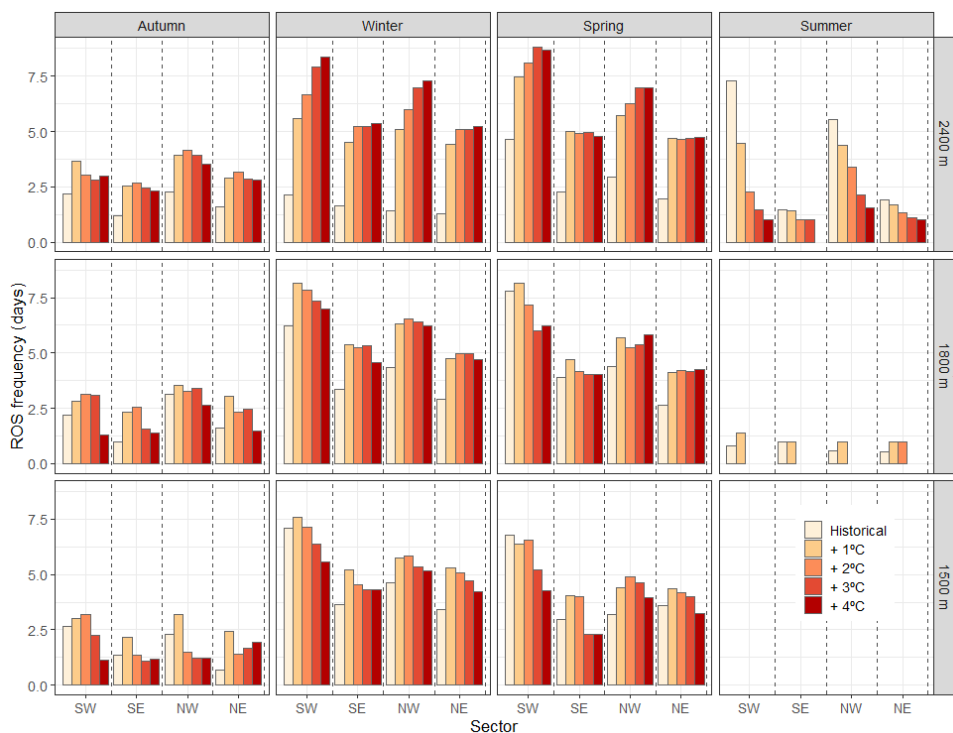
During the historical climate period, (1980 – 2019), the annual ROS frequency totals, on average, 10, 12 and 10 day/season for elevations of 1500 m, 1800 m, and 2400 m elevations. However, there are large differences depending on the sector. The annual ROS frequency at 1500 m elevation annual ROS frequency for the historical climate period is 17, 8, 10 and 7 days/year for SW, SE, NW, NE sectors, respectively (Figures 4 and S1). The highest annual ROS frequency is however observed simulated at 1800 m elevation. Here, annual ROS frequency where it is 17, 9, 12 and 9 for SW, SE, NW, NE sectors. Within 1500 m and 1800 m these elevations, the maximum ROS frequency is detected in the SW during winter and spring (7 days/season, for both elevations and seasons). The SE and NE eastern Pyrenees exhibit follow a similar seasonality. The maximum ROS frequency at 1500 m elevation is found in winter (4 and 3 days/season, for SE and NE,

296 respectively), and during spring at 1800 m elevation (4 and 3 days, for SE and NE, respectively). ROS is  
 297 rarely simulated observed in the SE during the latest month of spring (May), which contrast with the simulated  
 298 values for the SW (2 and 3 days/month, for 1500 m and 1800 m elevations, respectively). 2400 m elevation  
 299 shows the minimum ROS frequency. Here, comparisons Comparisons between seasons at 2400 m reveal the  
 300 maximum ROS frequency during summer, especially in the SW (7 days/season), followed by NW (6  
 301 days/season), and NE (2 days/season).

302  
 303  
 304



305  
 306

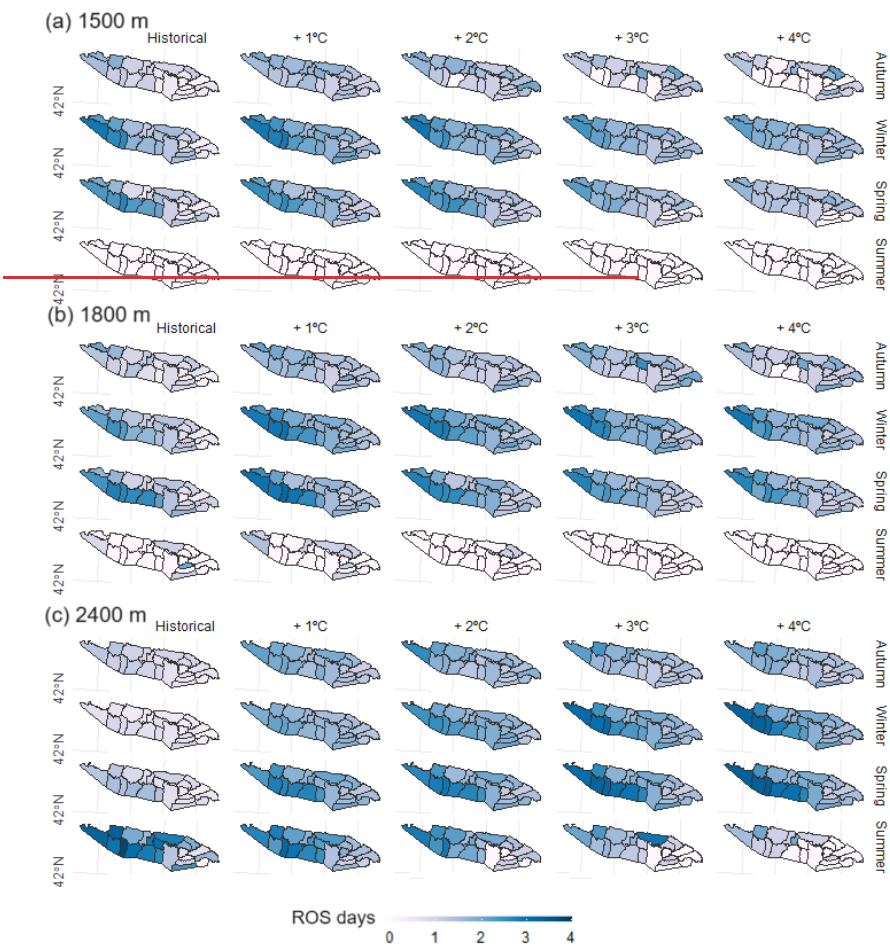


Con formato: Centrado

**Figure 4.** ROS frequency (days). Data are presented for the historical climate period (1980 – 2019) with different increments of temperature (colors), grouped by sector (x-axis), elevations and seasons (boxes). for the historical climate period (1980 – 2019) and increments of temperature (colors), grouped by months (x-axis), sector (rows) and elevation (columns). Data represent the average of the simulated precipitation change, ranging from -10% to 10%, by steps with increments of 10%.

The ROS frequency response to warming varies depending on the month, increment of temperature, elevation, and sector (Figures 4, 5 and S4). ROS tends to disappear in October at 1500 m elevation for  $\geq 1^\circ\text{C}$ , except in SW. (Figure 4 and 5). The highest increases are simulated during the winter for increments temperature lower than  $3^\circ\text{C}$ , particularly in NE, where ROS frequency increases by 1 day per month over the historical climate period for  $\pm 1^\circ\text{C}$ . ROS frequency progressively increases in March and April for all sectors but tends to decrease in May (for  $\geq 3^\circ\text{C}$ ), June and July (for  $\geq 1^\circ\text{C}$ ). At 1800 m elevation, ROS frequency increases in all regions from November to February (around 1 day per month, for  $\geq 1^\circ\text{C}$  up to  $\leq 3^\circ\text{C}$ ). At 1500 m, similar increases are expected in NW and SW during the earliest months of spring and for 1500 m to moderate increments of temperature for  $\leq 2^\circ\text{C}$  (Figure S4). The contrary is observed during Conversely, during the latest months of spring in SW, where warming reduces ROS events. A slight ROS frequency increase is found during spring for the rest of the sectors (Figure 4). In addition, ROS events in June are expected to disappear for temperature increases higher than  $1^\circ\text{C}$ . Finally, 2400 m elevation shows

326 the largest ROS frequency variations (around 1 day/month for  $\pm 1^\circ\text{C}$ ). Maximum ROS frequency increases  
 327 (3 days/month) are found in SW for more than  $+3^\circ\text{C}$ . ROS frequency progressively increases in March and  
 328 April for all sectors but tends to decrease in May (for  $+3^\circ\text{C}$ ), June and July (for  $+1^\circ\text{C}$ ).  
 329  
 330



331

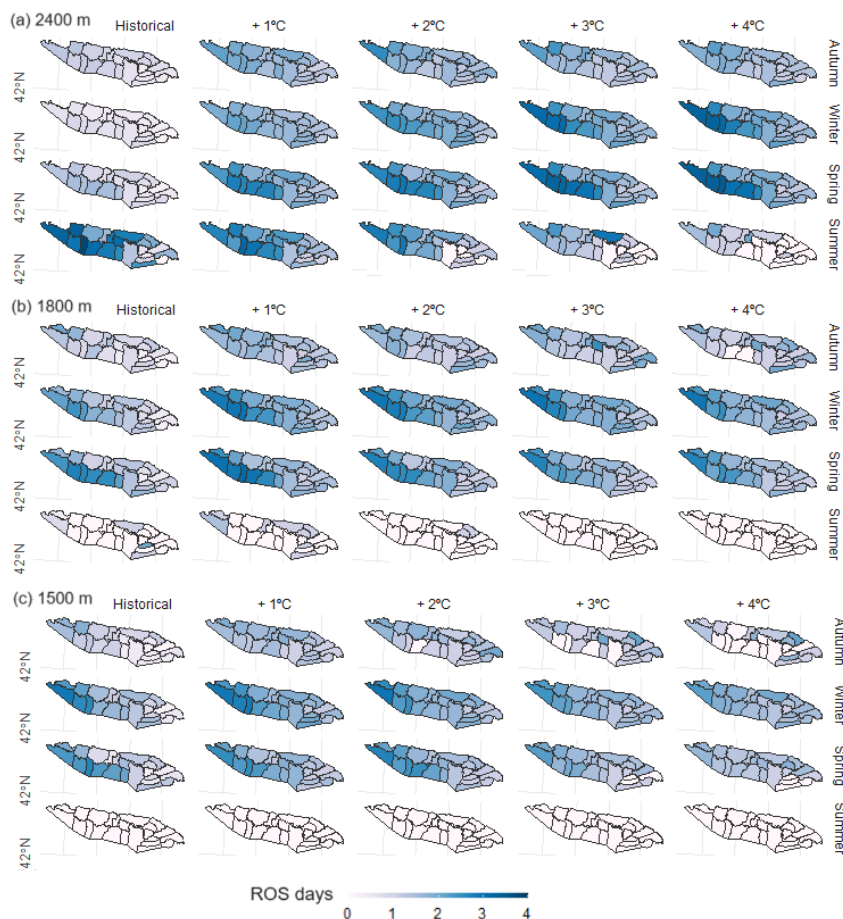
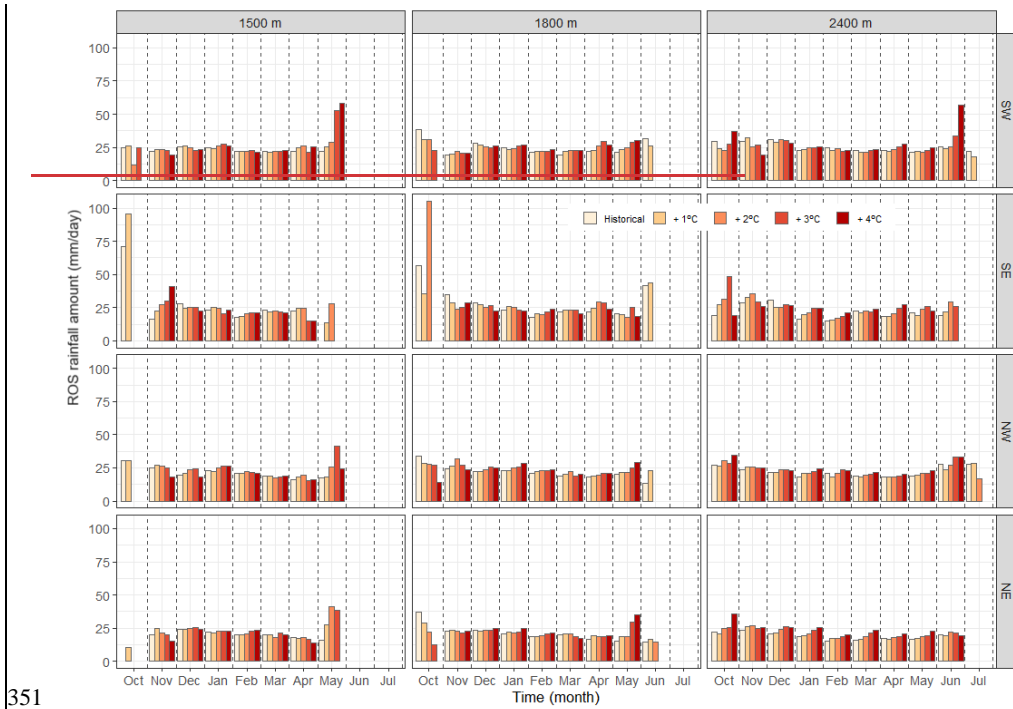


**Figure 5. Average ROS frequency (days) for a season for (a) 1500 m, (b) 1800 m, and (c) 2400 m elevations. Data are presented for the historical climate period (1980 – 2019), and increments of temperature (left to right) and seasons (rows). Data represent the average of the simulated precipitation change (ranging from -10% to 10%, by steps with increments of 10%).**

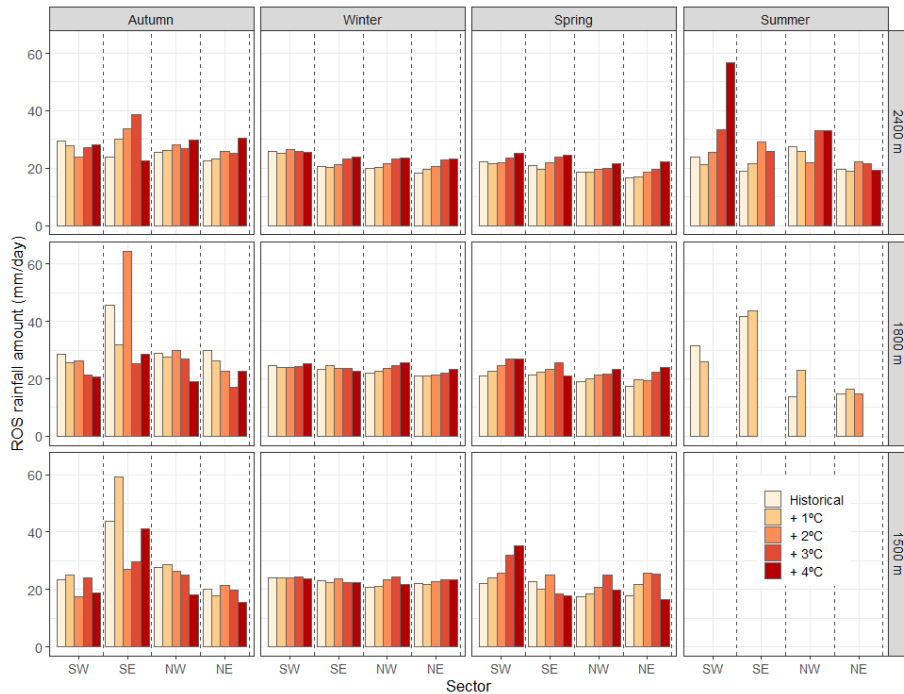
### 4.3 ROS rainfall amount

The spatial and temporal distribution of ROS rainfall amount is presented in Figures 6 and 7. The average ~~1500 m elevation~~ ROS rainfall amount at 1500 m elevation per year is 23, 28, 21, and 20 mm/day for SW, SE, NW, NE sectors, respectively. Similar values are found at 1800 m elevation, the highest ROS rainfall amount values are also found in SE (29 mm/day). Particularly, The SE sector experiences the highest ROS rainfall amount during autumn and summer (around 40 mm/day at 1500 m and 1800 m elevations). At 2400 m

345 elevation, however, the maximum ROS rainfall amount values are found in SW and NW during autumn. Here,  
 346 the largest ROS rainfall amount spatial and seasonal distribution ranges from SW (29 mm/day, autumn), NW  
 347 (28 mm/day, summer), SE (24 mm/day, autumn) to NE (23 mm/day, autumn).  
 348  
 349  
 350

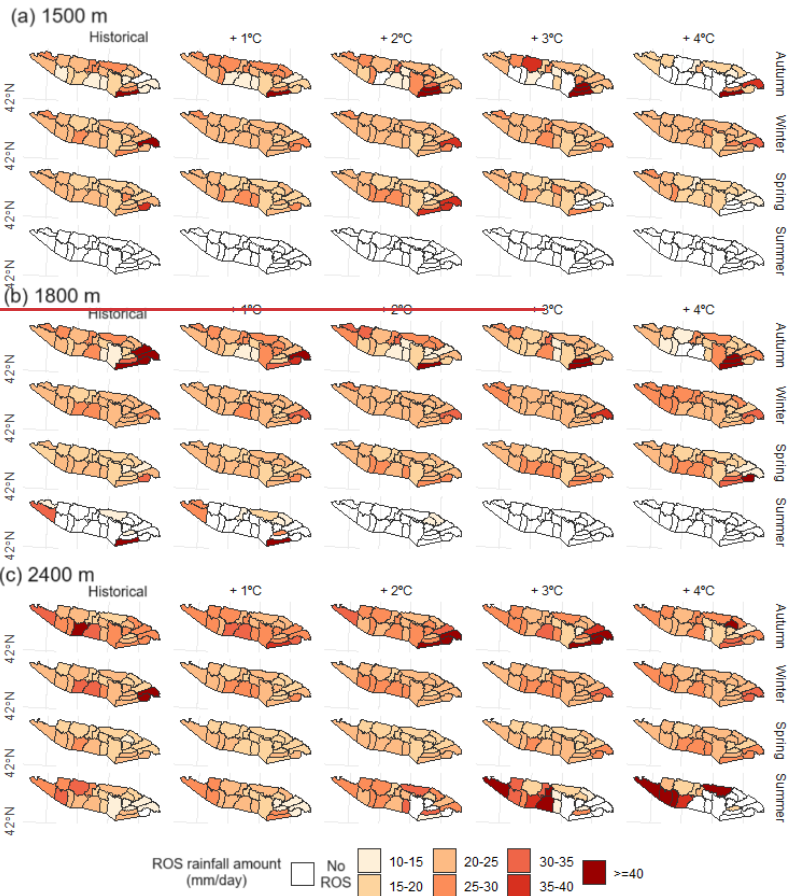


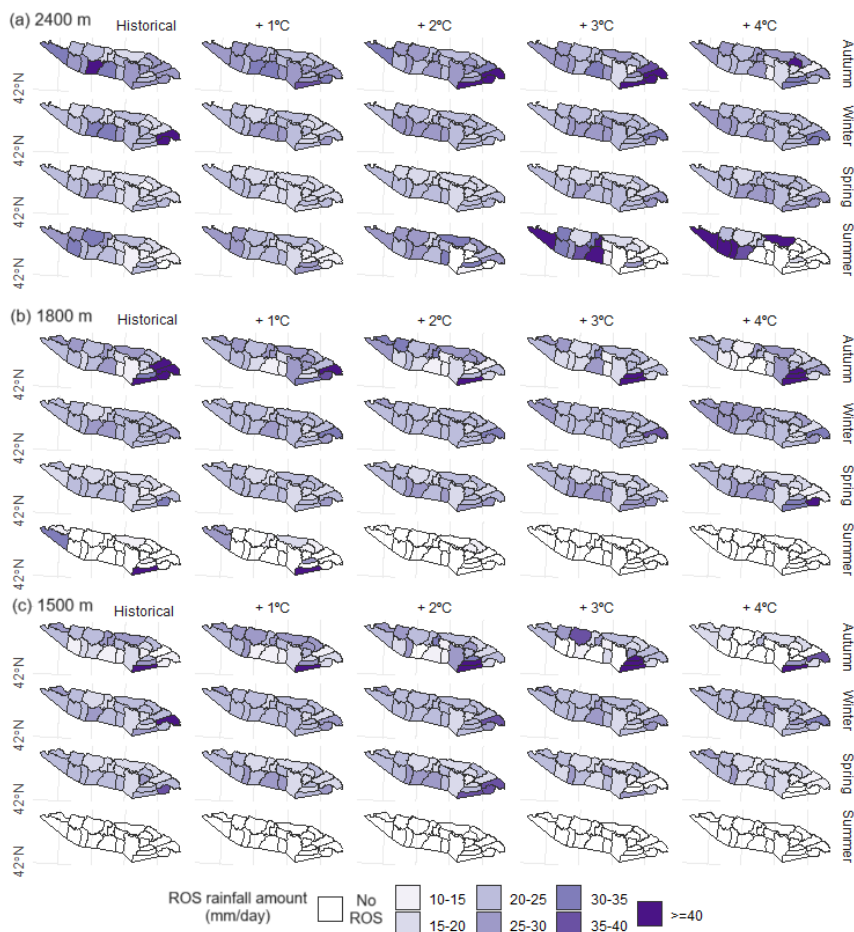




**Figure 6.** Average ROS rainfall amount (mm/day) for each month of the season. Data are shown-presented for the historical climate period (1980 – 2019) with-and different increments of temperature (colors), grouped by sector-month (x-axis), elevation and season-sector (boxes). Data represent the average of the simulated precipitation changes (ranging from -10% to 10%, with increments by steps of 10%).

ROS rainfall amount progressively increases due to warming (4%, 4%, and 5% per °C for 1500 m, 1800 m, and 2400 m elevations, respectively; Table S2). Small differences are found by elevation and sector. At 1500 m elevation, ROS rainfall amount increases until +3°C, and generally decreases for +4°C during the earliest (October to December) and latest (April and May) months of the snow season (Figure S5). Similar patterns are found at 1800 m elevation. ROS rainfall amount increases up to +4°C, except in the SE sector for specific months. (Figure 6). The latter sector shows also shows maximum ROS rainfall amount values in autumn due to torrential rainfall. At 2400 m elevation, ROS rainfall amount increases at a constant rate of around 5 % per °C. Yet, The maximum increases are simulated in SW during summer, when ROS rainfall amount almost doubles the historical climate period (+40% for +4°C).

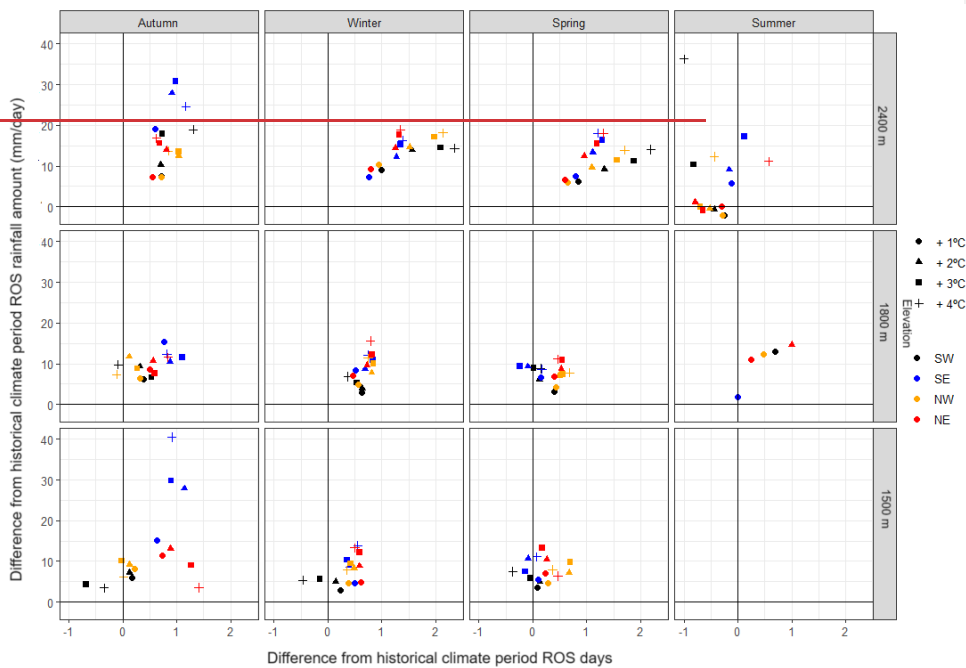




371  
 372 **Figure 7.** Average ROS rainfall amount (mm/day) ~~for a season (rows)~~ for (a) 1500 m, (b) 1800 m, and (c)  
 373 2400 m elevation. Data are shown for the historical climate period (1980 – 2019), ~~and~~ increments of  
 374 temperature (columns), ~~and seasons (rows)~~. Data represent the average of the simulated precipitation changes  
 375 (ranging from -10% to 10%, in increments of 10%).  
 376 Data are the average of the simulated precipitation change (from -10% to 10%, by steps of 10%).  
 377  
 378 For most sectors and elevations, the ROS frequency and ROS rainfall amount typically increase during winter  
 379 and early spring (Figure 8). The most important increases in ROS frequency and ROS rainfall amount are  
 380 simulated at 2400 m. Conversely, smaller changes in ROS frequency are observed at elevations of 1500 m and  
 381 1800 m, particularly with large increments in temperature, despite an expected increase in ROS rainfall amount  
 382 (< 10 mm/day). Similarly, during summer, ROS frequency generally decrease across all elevations due to

severe warming and snow cover depletion. Data suggest that ROS rainfall amount and frequency generally increases for all elevations and sectors during winter (except in SW for temperatures greater than 3°C) (Figure 8). Nonetheless, remarkable spatial and seasonal differences are found. SE shows the maximum values in autumn. On the contrary, small changes in frequency are detected in SW and NW, despite ROS rainfall amount is expected to increase (< 10 mm/day). For most sectors and elevations, ROS rainfall amount and frequency generally increases in winter and spring. The minimum differences between sectors are detected in these seasons. In summer, ROS rainfall amount and frequency tends to generally decrease for all elevations under severe warming due to snow cover depletion.

391  
392  
393



394

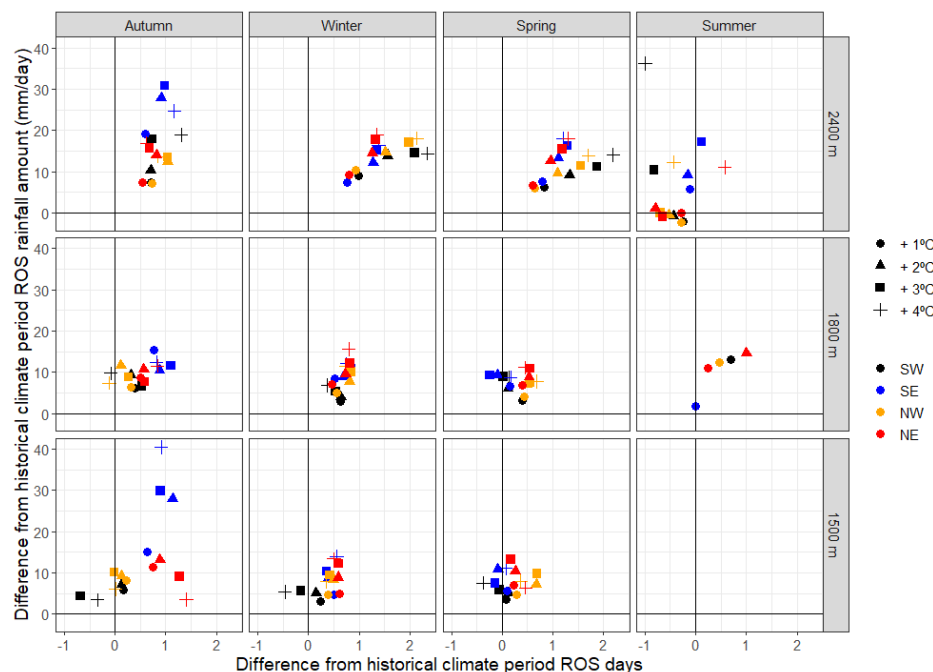


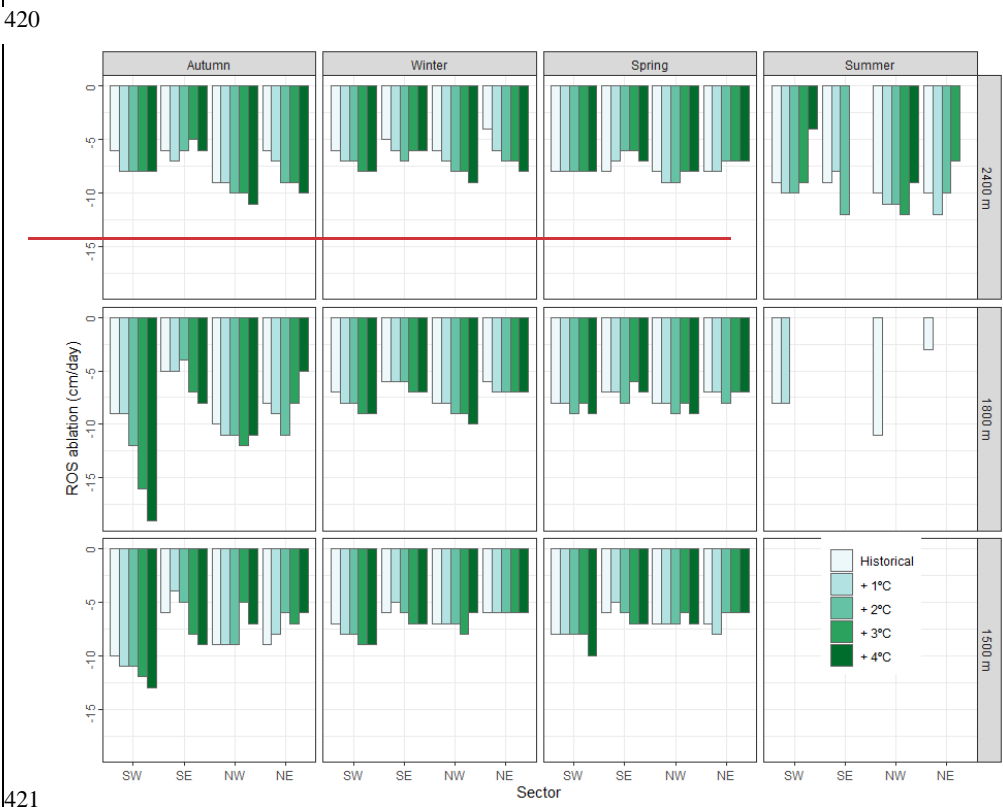
**Figure 8.** Scatterplot between ROS rainfall amount (mm/day) difference from the historical climate period (1980 – 2019) (y-axis) and ROS days difference from the historical climate period (x-axis). Data is calculated as the average difference between (a) the values of the historical climate period values and (b) the values resulting from the different increments of temperature, only for the massifs where ROS frequency exists in (a) and (b). Data are presented for each season (columns), elevation (rows), sector (color) and increment of temperature (point shape). Data represent the average of the simulated precipitation change (ranging from -10% to 10%, in increments by steps of 10%).

#### 4.4. ROS ablation

ROS ablation is presented in Figures 9, 10 and S6. ROS ablation ranges from -10 cm/day in NW at 2400 m elevation (summer) to -5 cm/day in NE at 2400 m elevation (winter). ROS ablation nearly doubles the average daily snow ablation for all days in a season (Figure S6). A comparison with the reference baseline-historical climate period reveals contrasting ROS ablation changes depending on the season, elevation, and sector. Overall, ROS ablation progressively increases due to warming in coldest zones and months of the season. The largest ROS ablation increments are detected in autumn and winter. For the former, ROS ablation in autumn increases at a generally constant rate in SW (11 %), NE (19 %) and NW (4 % per °C). For the latter, ROS ablation also increases during winter in SW (11 %), NW (14 %) and NE (34 % per °C). In detail, The maximum ROS ablation due to warming is found for 1800 m elevation during autumn

415 (Figure 9). ROS ablation exhibits slow and no-changes in the warmest zone (SE), as well as in the warmest  
416 months of the season, regardless of the elevation band.

Con formato: Izquierda



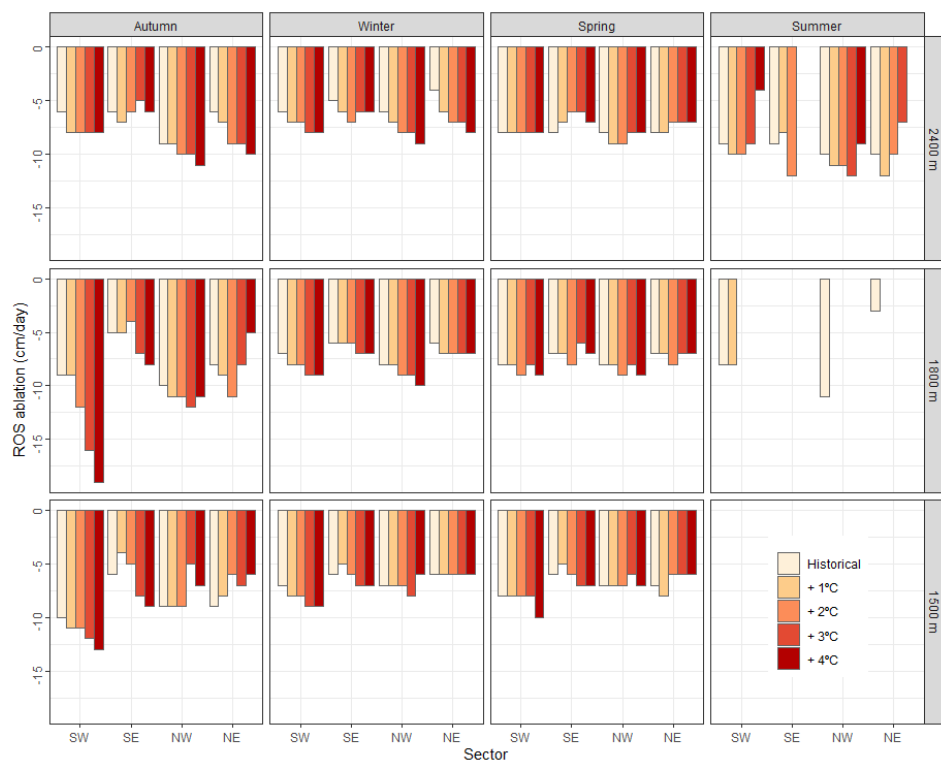
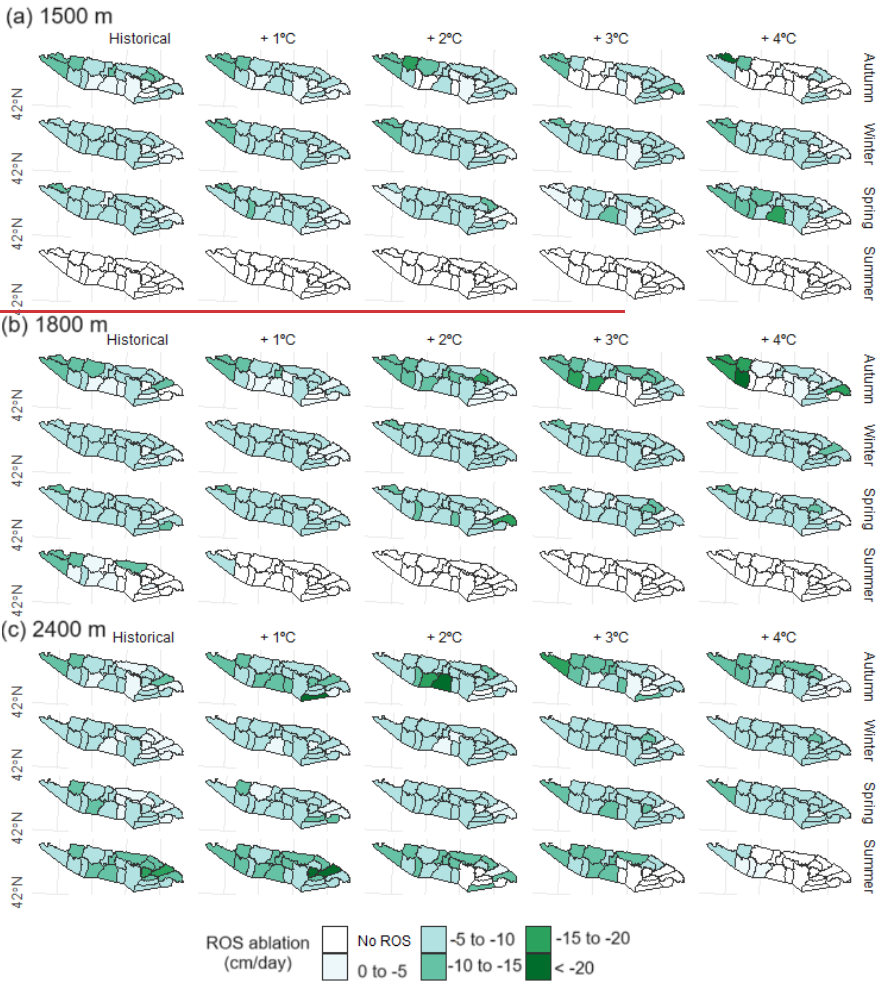


**Figure 9.** Average ROS ablation (cm/day) for the historical climate period (1980 – 2019) and increments of temperature (colors), sectors (x-axis), season (columns) and elevations (rows). Data represent the average of the simulated precipitation change (ranging from -10% to 10%, by steps of 10%).

427  
428  
429



430



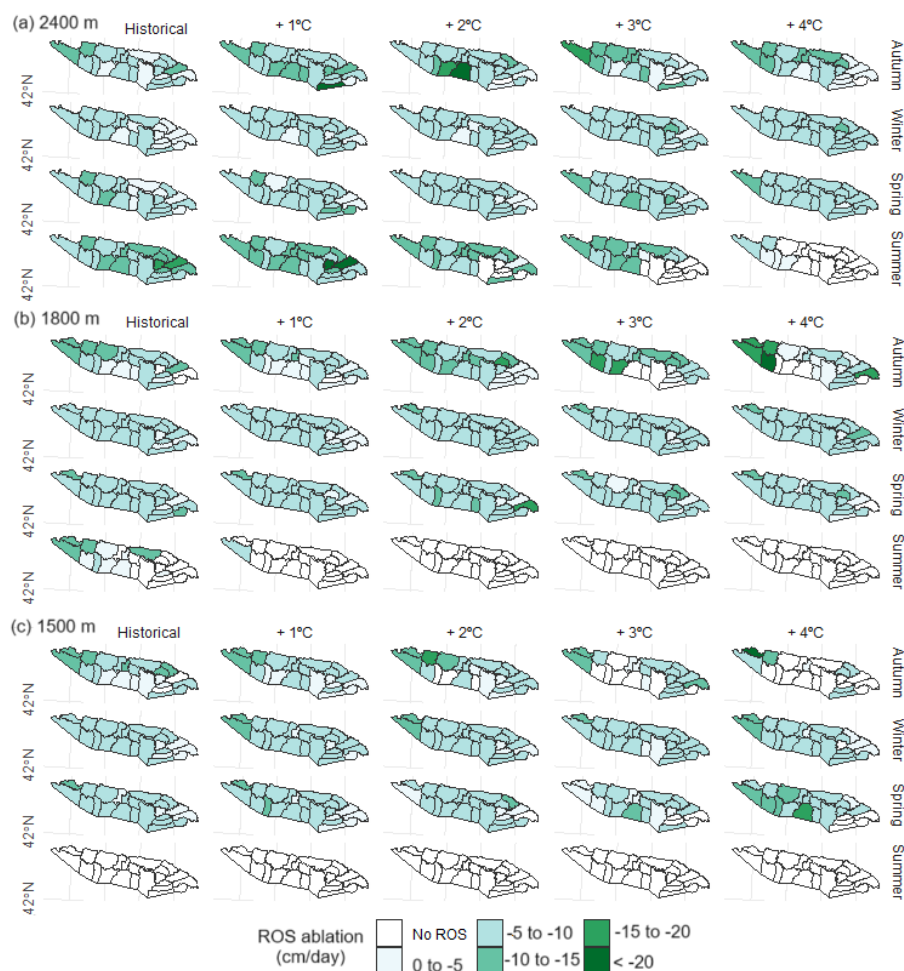


**Figure 10.** Average ROS ablation (cm/day) for (a) 1500 m, (b) 1800 m, and (c) 2400 m elevations. Data are shown for the historical climate period (1980 – 2019) and increments of temperature (columns) and seasons (rows). Data represent the average of the simulated precipitation change (ranging from -10% to 10%, by steps of increments of 10%).

## 5 Discussion

The Pyrenees experienced a statistically significant positive temperature trend. The temperature in the Pyrenees statistically significant increased since the 1980s from 1980 to 2015 (ca. + 0.2 °C/decade), although

442 ~~however but~~ no statistically significant precipitation trends ~~have been are~~ detected ~~for the same period~~ (OPCC,  
 443 2018). ~~This, which has been attributed due to the~~ strong spatial ~~variability~~ (Vicente-Serrano et al., 2017), ~~as~~  
 444 ~~well as~~ inter-annual and long-term variability ~~of precipitation of the latter~~ (Vicente-Serrano et al., 2017; Peña-  
 445 Angulo et al., 2021). ~~Similarly, Different snow trends have been identified~~ showed contrasting spatio-temporal  
 446 ~~patterns~~ depending on the study ~~temporal period and sector, different snow trends were found~~. From ~~around a~~  
 447 1980 to 2010, non-statistically significant ~~snow days and snow accumulation~~ positive trends were generally  
 448 ~~detected observed in snow days and snow accumulations~~ at ~~elevations~~ > 1000 m (Buisan et al., 2016), 1800 m  
 449 (Serrano-Notivoli et al., 2018), and > 2000 m (Bonsoms et al., 2021a). ~~However, Long-term trends~~ (1957 to  
 450 2017), ~~however, reveal~~ statistically significant ~~decreases in~~ snow depth ~~decreases~~ at 2100 m, ~~with but~~ large  
 451 variability depending on the sector and the snow indicator (López-Moreno et al., 2020). Climate projections  
 452 for the end of the 21<sup>st</sup> century suggest an increase of temperature (> 3°C), ~~together with coupled with small~~  
 453 ~~precipitation 1500 m precipitation~~ shifts (<= 10%) from autumn to spring (Amblar-Francés et al., 2020).  
 454 ~~In Within~~ this climate context, ~~spatial and temporal~~ ROS ~~spatio-temporal~~ patterns ~~are will~~ likely ~~to~~ change. ~~In~~  
 455 ~~order to To~~ anticipate future ROS patterns, we analyzed ROS sensitivity to warming through three key  
 456 indicators: ~~ROS of~~ frequency, rainfall ~~intensity amount~~ and ~~snow~~ ablation.

457

## 458 5.1 ROS spatial variability

459

460 ~~The climatic setting of the Pyrenees as well as its relief configuration determines a remarkable spatial and~~  
 461 ~~temporal variability of ROS events~~. HS decreases ~~by~~ 39 %, 37 % and 28 % per °C, for 1500 m, 1800 m, and  
 462 2400 m elevations, respectively. Similarly, Sf decreases by 29 %, 22 %, and 12 % per °C for 1500 m, 1800 m,  
 463 and 2400 m elevations. These results provide evidence of an elevation-dependent snow sensitivity to  
 464 temperature change and are consistent with snow sensitivity to climate works in near alpine sectors, such as  
 465 the Alps (e.g., Martin et al., 1994). HS and Sf ~~exhibit~~ maximum reductions ~~are reached for 1°C of warming,~~  
 466 suggesting non-linear HS decreases, in accordance with previous snow sensitivity to climate change reported  
 467 in ~~the~~ central Pyrenees (López-Moreno et al., 2013). The ~~generally reported increase in~~ ROS rainfall amount  
 468 ~~increase reported~~ in this work, independently of the increment of temperature and elevation, is explained by  
 469 the Sf reduction expected for all sectors (Figure 3). Large increments of warming decreases ROS frequency  
 470 due to snow cover depletion in early autumn and late spring (Figure 2). However, for the rest of the seasons,  
 471 and even with snow cover reductions, the snowpack does not fully disappear, leading to ROS frequency  
 472 increases due to more rainy days.

473

474 ~~The 2400 m elevation shows the largest variation over the historical climate period as well as ROS rainfall~~  
 475 ~~amount and frequency (Figure 8) because of the thicker snowpack and duration compared to 1500 m and 1800~~  
 476 ~~m areas. Thus, the 2400 m elevation snow duration last until spring and summer, when the largest shift from~~  
 477 ~~snowfall to rainfall is found. On the other hand, the 1800 m elevation shows the maximum ROS rainfall amount~~  
 478 ~~since the amount of moisture for condensation decreases while air masses increase height (Roe and Baker,~~  
 479 ~~2006).~~ SW and NW annual ROS frequency almost doubles (17 and 12 days/year, respectively) the ~~ROS~~

frequency one-recorded in SE and NE (9 days/year, for both sectors). The maximum ROS frequency for a season is found in SW and NW because of larger due to thicker snowpacks in this sector (i.e., López-Moreno, 2005; López-Moreno et al, 2007; Navarro-Serrano et al., 2017; Bonsoms et al., 2021a). Thus, snow cover lasts longer until spring when minimum Sf values are found (Figure 2). SW and NW sectors are the most exposed to SW and W air flows (negative NAO phases) (López-Moreno, 2005), which bring wet and mild conditions over the mountain range, leading to most ROS-related floods in the range (Morán-Tejeda et al., 2019). The maximum ROS rainfall amount is generally detected in May, except in NE (at 2400 m elevation) and SE (all elevations), where, in the latter sectors, ROS rainfall amount tends to disappear in October under large (> 2°C) increments of temperature. The seasonal snow accumulation in NE and SE the Eastern Pyrenees is lower-than-average due to the lower influence of Atlantic climate in these sectors of the range. In addition, the SE is closer to the 0°C due to higher-than-average sublimation, latent and radiative heat fluxes (Bonsoms et al., 2022) and for this reason in this sector each increment of temperature has larger effects on the Sf, HS and ROS frequency reduction (Figures 2 and 3). 2400 m elevation shows the largest variation over the historical climate period as well as ROS rainfall amount and frequency (Figure 8) because of the larger snowpack and duration compared to 1500 m and 1800 m areas. Thus, 2400 m elevation snow duration last until spring and summer, when the largest shift from snowfall to rainfall is found. On the other hand, 1800 m elevation shows the maximum ROS rainfall amount since the amount of moisture for condensation decreases while air masses increase height (Roe and Baker, 2006). The largest ROS rainfall amount is detected in SE during autumn (Figures 6, 7 and S5). This is because sector is exposed to Mediterranean low-pressure systems (negative WeMO phases), which that usually trigger heavy rainfall events during autumn (Lemus-Canovas et al., 2021) during this season, when snow cover may have already developed at a sufficiently high elevations sufficiently high elevation.

## 5.2 ROS Comparison with other studies

Recent ROS trends in other mid-latitude areas are in accordance align with ROS analysis presented here. Freudiger et al. (2013) analyzed the ROS trends- (1950 – 2011 period) of at the Rhine, Danube, Elbe, Weser, Oder, and Ems (Central Europe) basins for the period 1950 – 2011. They observed found an overall ROS frequency increase in ROS frequency during January and February from (1990 to 2011 period), which is consistent with the simulated increase in ROS rainfall amount and frequency increase simulated in winter for the Pyrenees across for all elevations and increment of temperature temperature increments range increases. Similarly, in the Sitter River (NE Switzerland), a ROS frequency increase of around 40% (at elevations below 1500 m) and 200% (at elevations above 2500 m) was detected from 1960 to 2015 (200%) at <1500 m (>2500 m) was detected between 1960 and 2015 (Beniston and Stoffel, 2016). In the Western United States, During the last half of the 20<sup>th</sup> century, ROS frequency trends showed an upward trend at high elevations and a downward trend at low elevations (downward trend in high (low) elevation in western United States (McCabe et al., 2007). Similar results were found at, as well as in southern British Columbia (Loukas et al., 2002) and in at catchment scale in Oregon (United States) (Surfleet and Tullos, 2013). Same ROS frequency increases

518 were detected from 1980 to 2010 in Norway at high-elevated mountain zones, while decreases were found at  
519 low-elevated zones (Pall et al., 2019). Same ROS frequency increases (decreases) has been detected from 1980  
520 to 2010 in Norwegian at high (low) elevated mountain zones (Pall et al., 2019). However, in contrast ~~stidiction to~~  
521 ~~with~~ our results and previous studies, at hemispheric scale, winter Northern-Hemisphere ROS frequency  
522 trends ~~during the (1979 -- 2014 period)~~ showed no clear trends (Cohen et al., 2015).

523  
524 Results ~~presented~~exposed in this work provide ~~furthermore~~ evidence of ROS frequency increases in high-  
525 elevation zones, ~~as it has been suggested by~~aligning with climate projections and studies on ROS sensitivity  
526 to temperature ~~studies~~. The elevation-dependent pattern of ROS, previously reported in the Swiss Alps (Morán-  
527 Tejada et al., 2016), is consistent with findings ~~in at the~~ Sitter River catchment (NE Switzerland), where a  
528 temperature increases of 2 to 4 °C over the 1960 ~~to~~ 2015 period resulted in a 50% increase in ROS frequency  
529 at elevations above 2500 m (Beniston and Stoffel, 2016). ROS shows an elevation-dependent pattern that was  
530 ~~previously reported in the Swiss Alps (Morán-Tejada et al., 2016). In Sitter River (NE Switzerland), an increase~~  
531 ~~of 2 to 4 °C over the 1960 to 2015 period results in an increase of the ROS frequency by around 50% at > 2500~~  
532 ~~m (Beniston and Stoffel, 2016). Likewise, 21<sup>st</sup> century high emission scenarios (RCP8.5), suggest increases in~~  
533 ~~ROS frequency and intensity in Gletsch (Switzerland) high elevation area. Other studies indicate that for~~  
534 ~~climate projections involving ROS definitions that include snow melting (Musselman et al., 2018), natural~~  
535 ~~climate variability contributes to a large extent (70%) of ROS variability (Schirmer et al., 2022). Other studies~~  
536 ~~suggest that on climate projections for ROS definitions that include snow melting (Musselman et al., 2018),~~  
537 ~~natural climate variability contributes to a large extend (70 %) of ROS variability (Schirmer et al., 2022). Li~~  
538 ~~et al. (2019) analyzed the future ROS frequency in the conterminous United StatesUnited States- and detected~~  
539 a nonlinear trend in ROS events due to warming, ~~which is~~ consistent with the ~~different-varied~~ ROS rainfall  
540 amount and frequency responses ~~simulated depending on the increment of temperature detected~~ in our work  
541 based on different temperature increments. Climate projections for the mid-end of the 21<sup>st</sup> century ~~projected~~  
542 indicate positive ROS frequency and rainfall trends in Western ~~United StatesUnited States-~~ and Canada (il  
543 Jeong and Sushama, 2018). Similarly, ROS frequency is projected to decrease in the warmest months of the  
544 season in low elevation areas of Western United States, but increase at high elevations ~~will likely decrease~~  
545 ~~(increase) in the warmest months of the season in low (high) elevation areas of western United States~~  
546 (Musselman et al., 2018). The same trend is projected for Norwegian mountains (Mooney and Li, 2021).  
547 López-Moreno et al. (2021) analyzed ~~40 worldwide basins~~ ROS sensitivity to warming in 40 worldwide basins  
548 ~~and- In theirTheir study they~~ found a decrease in ROS events in warm mountain areas. However, they  
549 detected ROS frequency increases in cold-climate mountains ~~whithere~~ large snow accumulation ~~is found~~  
550 despite warming. ~~In accoordance-~~ Consistent with our results, they identified large seasonal differences and  
551 ROS frequency decreases in Mediterranean mountains due to snow cover depletion in the last ~~s~~ months of the  
552 snow season.

553

### 554 5.3 ROS ablation

555 Warming increases ROS ablation from autumn to winter ~~on~~ in deep snowpacks and in the coldest sectors of  
556 the range. ~~This is attributed, due to the~~ higher energy for snow ablation and ~~the conditions~~ closer ~~to the~~ 0°C  
557 isotherm ~~conditions in a warmer than~~ compared to the historical climate period. ~~Data show no~~ changes and  
558 decreases in ROS ablation in ~~the SE during~~ and spring since the snowpack is already near to the isothermal  
559 conditions. These ~~results go in line~~ findings are consistent with results ~~simulated~~ observed in both ~~for~~ cold and  
560 warm Pyrenean sites (López-Moreno et al., 2013), ~~and as well as for different~~ Northern-Hemisphere sites  
561 (Essery et al., 2020). ~~The~~ ROS ablation indicator is ~~also~~ indirectly affected by the ~~HS~~ magnitude decreases in  
562 HS (30 % per °C; Figure 3), ~~and therefore lower~~ resulting in lower ROS ablation ~~is directly affected by lower~~  
563 ~~HS magnitudes~~. Previous literature ~~pointed out that warming have different~~ has highlighted the diverse effects  
564 of warming on snow ablation patterns. Higher ~~than~~ average temperatures advance the peak HS date ~~by~~ on  
565 average of 5 days per °C in elevations of 1800 m and 2400 m ~~elevations~~ (Bonsoms et al., 2023a), leading to  
566 ~~triggering earlier onsets of~~ snow ablation ~~on onsets, and therefore and lower~~ solar radiation fluxes (López-  
567 Moreno et al., 2013; Lundquist et al., 2013; Pomeroy et al., 2015; Musselman et al., 2017a; Sanmiguel-  
568 Vallengado et al., 2022), ~~and earlier depletion of snow as well as earlier snow depletion~~ before the maximum  
569 advection of heat fluxes into the snowpack ~~(spring)~~ (Bonsoms et al., 2022). Slower snow-melt rates in a warmer  
570 climate have been detected in Western ~~United States~~ United States (Musselman et al., 2017), ~~as well as the~~  
571 ~~entire and across the entire~~ Northern ~~Hemisphere~~ (Wu et al., 2018). Low or ~~non~~ inexistent changes in snow  
572 ablation on warm and marginal snowpacks ~~have~~ been previously detected in the Central Pyrenees (López-  
573 Moreno et al., 2013), in forest and open areas (Sanmiguel-Valellado et al., 2022), across ~~in~~ the entire range  
574 (Bonsoms et al., 2022), and in other mountain ranges in the Iberian mountain ranges Peninsula outside the  
575 Pyrenees and other Iberian Peninsula Mountain ranges outside the Pyrenees (Alonso-González et al., 2020a).

576 ROS ablation is larger than the average snow ablation during a snow ablation day (Figure S65) due to higher  
577 SEB positive fluxes. Several ~~works analyzed have examined~~ SEB ~~changes during~~ on ROS events, ~~and~~  
578 ~~different revealing varying~~ SEB contributions ~~has been found depending based~~ on the geographical area  
579 (Mazurkiewicz et al., 2008; Garvelmann et al., 2014b; Würzer et al., 2016; Corripio and López-Moreno, 2017;  
580 Li et al., 2019). The energy available for melting during ROS days range ~~ranging~~ from net radiation in Pacific  
581 North West (Mazurkiewicz et al., 2008) to LWin and turbulent heat fluxes in mountain areas of the  
582 conterminous ~~United States~~ United States mountain areas (Li et al., 2019) or the Swiss Alps (e.g., Würzer et  
583 al., 2016). In general, studies in mid-latitude mountain ranges have ~~shown~~ indicated that turbulent heat fluxes  
584 contribute between 60 and 90 % of the energy available for snow ablation during ROS days (e.g., Marks et al.,  
585 1998; Garvelmann et al. 2014; Corripio and López-Moreno, 2017). ~~In the central Pyrenees (at > 2000 m) the~~  
586 ~~the~~ The meteorological analysis of a ROS event in the Central Pyrenees (at > 2000 m) revealed that ROS ablation  
587 exceeds that of a normal ablation day due to the substantial advection of LWin and, especially, sensible heat  
588 fluxes (Corripio and López-Moreno, 2017). LWin increases owing to high cloud cover and warm air,  
589 commonly observed during ROS events (Moore and Owens, 1984). Future research should analyze the SEB  
590 controls during ROS events across the entire mountain range, as well as the hydrological responses of ROS to

climate warming, reveals that ROS ablation is larger than a normal ablation day because of the large advection of LWin and especially sensible heat fluxes (Corripio and López Moreno, 2017). LWin increases due to the high cloud cover and warm air, as it is frequently observed during ROS episodes (Moore and Owens, 1984). Further works should analyze the SEB controls during ROS events within the entire mountain range, as well as the ROS hydrological responses to climate warming.

#### 5.4 ROS socio-environmental impacts and hazards

Temperature-induced changes in the seasonal snowpack and during ROS days suggest various ~~several~~ remarkable hydrological shifts, including ~~but not limited to~~, earlier peak flows ~~in the season~~ (Surfleet and Tullos, 2013), rapid streamflow peaks during high precipitation events in frozen soils (Shanley and Chalmers, 1999), ~~accelerated soil moisture depletion, and reduced river discharges in spring due to earlier snowmelt in the season (Stewart, 2009). faster soil moisture depletion and lower river discharges in spring due to earlier snow melt in the season (Stewart, 2009).~~ The shortening of the snow season due to warming, as reported in this work, ~~will potentially~~ has also the potential to alter alpine phenological patterns (i.e., Wipf and Rixen, 2010) and expand forest cover (Szczypka et al., 2015). Although vegetation branches intercept a large amount of snowfall, intermediate and high vegetation shields short-wave radiation, ~~reduces, diminish~~ snow wind ~~transport and~~ transport and reduce turbulent heat fluxes (López-Moreno and Latron, 2008; Sanmiguel-Valellado et al., 2022).

~~Snow forest interactions, their sensitivity to climate change as well as the ROS hydrological response within a changing landscape is far from understood across the range and should be the base of forthcoming works.~~

The higher ROS rainfall amount and frequency (Figure 8) ~~are~~ will likely to result in increased hazards and impacts in the mountain ecosystem ~~imply an increase of ROS related hazards and impacts in the mountain ecosystem.~~ Heavy ROS rainfall amounts ~~changes alter~~ snow metamorphism on saturated snowpacks, ~~and~~ leadings to high-speed rapid water percolation (Singh et al., 1997). ~~The s~~ Subsequent water refreezing ~~changes alters the snowpack conditions, creating and creates~~ an ice-layer in the snowpack that ~~can may~~ reach the surface (Rennert et al., 2009). ROS events can cause plant damage (Bjerke et al., 2017), and the ice encapsulation of vegetation in tundra ecosystems can trigger severe wildlife impacts, ~~such as including~~ starvation among vertebrate herbivores ~~starvation, reindeer population mortality (Kohler and Aanes, 2004) and higher competition between species (Hansen et al 2014).~~ ~~Nevertheless, However, to date, no study has analyzed ROS-related impacts within a changing climate and its impacts any study to the date analyzed ROS related impacts~~ in flora and fauna across ~~s~~ Southern-European mountains.

Snow albedo decay due to positive heat fluxes and rainfall in ROS events (Corripio and López-Moreno, 2017), leads to faster snow ablation, even ~~in~~ on the ~~next subsequent~~ days (e.g., Singh et al. 1997). The combination of changes in internal snowpack processes, increased larger ROS rainfall amount, and more energy for snow

627 ~~ablation to ablate snow~~, during spring could enhance snow runoff, especially during warm and wet snowpack  
628 conditions (Würzer et al., 2016). In snow-dominated regions, ROS can lead to a specific type of avalanching  
629 (Conway and Raymond, 1993) and floods (Surfleet and Tullos, 2013). The latter ~~represents are~~ the most  
630 environmentally ~~ly~~ damaging risk in Spain (Llasat et al., 2014), ~~with and~~ around 50% of the floods ~~s~~ in the Iberian  
631 Peninsula ~~are due to~~ attributed to ROS events (Morán-Tejeda et al., 2019). ~~More than~~ Over half of the historical  
632 (1940 to 2012) flood events in the Ésera ~~R~~iver catchment (~~C~~entral Pyrenees) occurred during spring  
633 (Serrano-Notivol et al., 2017), ~~which coincide~~ coinciding with the snow ablation season. ROS floods have  
634 ~~also~~ economic impacts ~~ss~~. For instance ~~example~~, a ROS flood event ~~on that occurred on 13<sup>th</sup> June of (2013)~~ in  
635 the Garonne River (Val d'Aran, ~~C~~entral Pyrenees) cost approximately 20 million ~~of~~ euros to the public  
636 insurance (Llasat et al., 2014).

637

## 638 5.5 Limitations

639

640 This study ~~assesses~~ evaluates the sensitivity of ROS responses to ~~climate change, temperature and precipitation~~  
641 ~~changes~~, ~~enhancing~~ enabling a better ~~our~~ understanding of the non-linear ROS spatio-temporal variations in  
642 different sectors and elevations of the Pyrenees. Instead of presenting diverse outputs from climate model  
643 ensembles (López-Moreno et al., 2010), we provide ROS sensitivity values per 1°C, ~~making them~~ allowing for  
644 ~~comparability with other regions and seasons~~, ~~comparable to other regions and seasons~~. The temperature and  
645 precipitation change values used in this sensitivity analysis are based on established climate projections for the  
646 region (Amblar-Francés et al., 2020). ~~However, P~~precipitation projections in the Pyrenees ~~, however,~~ exhibit  
647 high uncertainties among different models, emission scenarios, and temporal periods (López-Moreno et al.,  
648 2008).

649

650 The SAFRAN meteorological system used in this work relies on a topographical spatial division and exhibits  
651 and accuracy of around 1 °C in air temperature and ~~approximately around~~ 20 mm in ~~the~~ monthly cumulative  
652 precipitation (Vernay et al., 2022). Precipitation phase partitioning methods are subject to uncertainties under  
653 close-to-isothermal conditions (Harder and Pomeroy, 2014). Hydrological models are also ~~prone~~ subject to  
654 errors in ~~the~~ snowpack prediction (Essery, 2015). However, the FSM2 is a multiphysics snowpack model that  
655 has been validated previously in the Pyrenees (Bonsoms et al., 2023) and compared against different snowpack  
656 models (Krinner et al., 2018), providing evidence of its robustness.

657

## 658 6 Conclusions

659 The ~~expected decreases~~ anticipated reductions in snowfall fraction (~~SF~~) and height of snow (~~HS~~) due to climate  
660 warming ~~are likely to will likely change~~ alter ROS spatio-temporal patterns across the Pyrenees, ~~and t~~  
661 ~~Th~~thus, therefore, a better comprehensive understanding of ROS is ~~of interest~~ required ~~needed~~ to anticipate future  
662 ~~climate and environmental conditions~~. This ~~study work~~ analyzed ~~the~~ ROS sensitivity to ~~warming temperature~~  
663 by ~~forcing using~~ a physically ~~-~~based snow model with perturbed reanalysis climate data (1980 – 2019 period)



664 for ~~elevation areas at~~ 1500 m, 1800 m, and 2400 m ~~elevation areas of the in the~~ Pyrenees. ROS sensitivity to  
665 temperature ~~and precipitation is evaluated assessed based on by~~ frequency, rainfall intensity, and snow ablation,  
666 ~~during ROS days.~~

667 ~~During-Throughout~~ the historical climate period, ~~the~~ annual ROS frequency ~~totals on average averages~~ 10, 12  
668 and 10 days/season for ~~elevations at~~ 1500 m, 1800 m, and 2400 m, ~~respectively. Higher-than-average annual~~  
669 ~~ROS frequencies are simulated at 1800 m elevation in SW (17 days/year) and NW (12 days/year), contrasting~~  
670 ~~with the minimum detected in SE (9 days/year). Overall, ROS frequency decreases during summer at 2400 m~~  
671 ~~elevation for temperatures exceeding 1°C. When temperature is progressively increased, the greatest ROS~~  
672 ~~frequency increases are found for SW at 2400 m elevation (around 1 day/month per °C. elevations. Higher-~~  
673 ~~than average annual ROS frequency are found in 1800 m elevation SW (17 days/year) and NW (12 days/year),~~  
674 ~~which contrast with the minimums detected in SE (9 days/year). The different spatial and seasonal ROS~~  
675 ~~response to warming suggest that contrasting and shifting trends could be expected in the future. Overall ROS~~  
676 ~~frequency decreases during summer at 2400 m elevation for > 1°C. When temperature is progressively~~  
677 ~~increased the greatest ROS frequency increases are found for SW 2400 m elevation (around 1 day/month for~~  
678 ~~+1°C). ROS frequency is highly sensitive to warming during in the snow onset and offset months when~~  
679 ~~diverging various factors play a key role come into play. On the one hand, maximum Sf decreases due to~~  
680 ~~warming are simulated for spring, leading to rainfall increases. On the other hand, warming depletes the~~  
681 ~~snowpack in the warmest and snow-driest sectors of the range. Consequently, data-results suggest a general~~  
682 ~~decrease in ROS frequency decrease for most of the SE massifs, where the snowpack is near the isothermal~~  
683 ~~conditions in the historical climate period. Yet, During spring, the highest ROS frequency increases are~~  
684 ~~detected simulated in SW and NW sectors, assume these sectors are less exposed to radiative and turbulent~~  
685 ~~heat fluxes and record record higher-than-average seasonal snow accumulations.~~

686 ROS rainfall amount generally increases due to warming, ~~independently regardless~~ of the sector and elevation,  
687 ~~although it is constrained by the number of ROS days being limited by the number of ROS days.~~ The ~~largest~~  
688 ~~most substantial~~ and constant increments are ~~observed simulated~~ in spring, ~~with then~~ ROS rainfall amount  
689 ~~increases rising at a rates of 7 %, 6 % and 3 % per °C for 1500 m, 1800 m, and 2400 m, respectively. The~~  
690 ~~increase in ROS rainfall amount increases~~ is influenced by Sf reductions, which decrease at ~~a rates~~ of 29 %,  
691 22 %, and 12 % per °C for 1500 m, 1800 m, and 2400 m elevations, respectively. ~~The maximum values of ROS~~  
692 ~~rainfall amount maximum values~~ are detected in SE (28 mm/day), especially ~~at in~~ 1800 m elevation during  
693 autumn (45 mm/day), ~~assume~~ this sector is exposed to subtropical Mediterranean flows.

694 Finally, ROS ablation ~~exhibits shows~~ contrasting patterns depending on the season, sector and elevation.  
695 Generally, ROS ablation increases in cold snowpacks, such as those simulated ~~at in~~ 2400 m elevation and during  
696 cold seasons (autumn and winter). ~~In these cases. Here,~~ ROS ablation follows a constant ablation rate of around  
697 + 10% per °C, ~~due to higher than average positive sensible and LW in heat fluxes.~~ However, in ~~the~~ SE and ~~at~~  
698 1500 m elevation, where marginal and isothermal snowpacks are found, no changes or decreases in ROS  
699 ablation are detected due to snowpack reductions in a warmer climate. ~~These R~~ results demonstrate the high



700 ~~snow~~-sensitivity of snow to climate within a mid-latitude mountain range and suggest significant changes with  
701 regards to water resources management. ~~Relevant implications in the ecosystem and socio-economic activities~~  
702 ~~associated with snow cover are anticipated.~~

#### 703 Data availability

704 The FSM2 is an open-access snow model (Essery, 2015) provided at <https://github.com/RichardEssery/FSM2>  
705 (last accessed on 15 January 2023). The SAFRAN climate dataset (Vernay et al., 2022) is available ~~throughby~~  
706 AERIS at <https://www.aeris-data.fr/landing-page/?uuid=865730e8-edeb-4c6b-ac58-80f95166509b#v2020.2>  
707 (last accessed on 16 December 2022). ~~Data of this work is are~~ available upon request ~~fromby~~ the first author  
708 ([josepbonsoms5@ub.edu](mailto:josepbonsoms5@ub.edu)).

#### 709 Author contribution

710 J.B., J.I.L.M., and E.A.G. designed the work. J.B. analyzed the data and wrote the manuscript. J.B., J.I.L.M.,  
711 E.A.G., C.D.B., and M.O. provided feedback and edited the manuscript. J.I.L.M., M.O. supervised the project  
712 and acquired funding.

#### 713 Competing interests

714 The authors declare that they have no conflict of interest.

#### 715 Disclaimer

716 We utilized DeepL (<https://www.deepl.com>) to correct grammar in certain sentences of the manuscript.

Con formato: Fuente: 11 pto, Negrita, Sin Cursiva

Con formato: Fuente: 11 pto, Sin Cursiva

#### 717 Acknowledgements

718 This work frames within the research topics examined by the research group “Antarctic, Artic, Alpine  
719 Environments-ANTALP” (2017-SGR-1102) funded by the Government of Catalonia, HIDROIBERNIEVE  
720 (CGL2017-82216-R) and MARGISNOW (PID2021-124220OB-I00), from the Spanish Ministry of Science,  
721 Innovation and Universities. JB is supported by a pre-doctoral University Professor FPI grant (PRE2021-  
722 097046) funded by the Spanish Ministry of Science, Innovation and Universities. The authors are grateful to  
723 Pascal Haegeli, Samuel Morin and an anonymous reviewer for their review of this manuscript.

#### 724 725 References

726  
727 Alonso-González, E., Aalstad, K., Baba, M. W., Revuelto, J., López-Moreno, J. I., Fiddes, J., et al. MuSA: The  
728 Multiscale Snow Data Assimilation System (v1.0). Geoscientific Model Development Discussions, 1–43.  
729 <https://doi.org/10.5194/gmd-2022-137>, 2022.  
730  
731 Alonso-González, E., López-Moreno, J.I., Navarro-Serrano, F., Sanmiguel-Valladolid, A., Aznárez-Balta, M.,  
732 Revuelto, J., and Ceballos, A.: Snowpack Sensitivity to Temperature, Precipitation, and Solar Radiation

733 Variability over an Elevational Gradient in the Iberian Mountains, *Atmos. Res.*, 243, 104973 [https://doi.org/](https://doi.org/10.1016/j.atmosres.2020.104973)  
734 10.1016/j.atmosres.2020.104973, 2020a.  
735  
736 Alonso-González, E., López-Moreno, J.I., Navarro-Serrano, F., Sanmiguel-Vallelado, A., Revuelto, J.,  
737 Domínguez-Castro, F., and Ceballos, A.: Snow climatology for the mountains in the Iberian Peninsula using  
738 satellite imagery and simulations with dynamically downscaled reanalysis data, *International Journal of*  
739 *Climatology*, 40(1), 477–491, <https://doi.org/10.1002/joc.6223>, 2019.  
740  
741 Alonso-González, E., López-Moreno, J. I., Navarro-Serrano, F. M., and Revuelto, J.: Impact of North Atlantic  
742 Oscillation on the snowpack in Iberian Peninsula mountains, *Water (Switzerland)*, 12,  
743 <https://doi.org/10.3390/w12010105>, 2020b.  
744 Amblar-Francés, M. P., Ramos-Calzado, P., Sanchis-Lladó, J., Hernanz-Lázaro, A., Peral-García, M. C.,  
745 Navascués, B., Domínguez-Alonso, M., Pastor-Saavedra, M. A., and Rodríguez-Camino, E.: High resolution  
746 climate change projections for the Pyrenees region, in: *Advances in Science and Research*, 191–208,  
747 <https://doi.org/10.5194/asr-17-191-2020>, 2020.  
748  
749 Beniston, M. and Stoffel, M.: Rain-on-snow events, floods and climate change in the Alps: Events may increase  
750 with warming up to 4 °C and decrease thereafter, *Science of the Total Environment*, 571, 228–236,  
751 <https://doi.org/10.1016/j.scitotenv.2016.07.146>, 2016.  
752 Beniston, M., Farinotti, D., Stoffel, M., Andreassen, L. M., Coppola, E., Eckert, N., Fantini, A., Giacona, F.,  
753 Hauck, C., Huss, M., Huwald, H., Lehning, M., López-Moreno, J. I., Magnusson, J., Marty, C., Morán-Tejeda,  
754 E., Morin, S., Naaim, M., Provenzale, A., Rabatel, A., Six, D., Stötter, J., Strasser, U., Terzago, S., and Vincent,  
755 C.: The European mountain cryosphere: A review of its current state, trends, and future challenges,  
756 <https://doi.org/10.5194/tc-12-759-2018>, 2018.  
757 Bieniek, P. A., Bhatt, U. S., Walsh, J. E., Lader, R., Griffith, B., Roach, J. K., and Thoman, R. L.: Assessment  
758 of Alaska rain-on-snow events using dynamical downscaling, *J Appl Meteorol Climatol*, 57, 1847–1863,  
759 <https://doi.org/10.1175/JAMC-D-17-0276.1>, 2018.  
760 Bonsoms, J., Franch, F. S., and Oliva, M.: Snowfall and snow cover evolution in the eastern pre-pyrenees (Ne  
761 iberian peninsula), *Geographical Research Letters*, 47, 291–307, <https://doi.org/10.18172/cig.4879>, 2021b.  
762 Bonsoms, J., González, S., Prohom, M., Esteban, P., Salvador-Franch, F., López-Moreno, J. I., and Oliva, M.:  
763 Spatio-temporal patterns of snow in the Catalan Pyrenees (NE Iberia), *International Journal of Climatology*,  
764 41, 5676–5697, <https://doi.org/10.1002/joc.7147>, 2021a.  
765 Bonsoms, J., López-Moreno, J. I., González, S., and Oliva, M.: Increase of the energy available for snow  
766 ablation in the Pyrenees (1959–2020) and its relation to atmospheric circulation, *Atmos Res*, 275,  
767 <https://doi.org/10.1016/j.atmosres.2022.106228>, 2022.  
768 Bonsoms, J., López-Moreno, J. I., and Alonso-González, E.: Snow sensitivity to temperature and precipitation  
769 change during compound cold–hot and wet–dry seasons in the Pyrenees, *The Cryosphere*, 17, 1307–1326,  
770 <https://doi.org/10.5194/tc-17-1307-2023>, 2023b.  
771 Bonsoms, J., Ninyerola, M. Comparison of linear, generalized additive models and machine learning  
772 algorithms for spatial climate interpolation, *Theoretical and Applied Climatology*, Preprint.  
773 <https://doi.org/10.1007/s00704-023-04725-5>, 2023a.

774 Buisan, S.T., López-Moreno, J.I., Sanz, M.A. and Korchendorfer, J. Impact of weather type variability on  
775 winter precipitation, temperature and annual snowpack in the Spanish Pyrenees. *Climate Research*, 69, 79–92.  
776 <https://doi.org/10.3354/cr01391>, 2016.

777 Bjerke JW, Treharne R, Vikhamar-Schuler D, Karlsen S R, Ravolainen V, Bokhorst S, Phoenix G K, Bochenek  
778 Z and Tømmervik H 2017 Understanding the drivers of extensive plant damage in boreal and Arctic  
779 ecosystems: insights from field surveys in the aftermath of damage *Sci. Total Environ.* 599 1965–76.

780 Cohen, J., Ye, H., and Jones, J.: Trends and variability in rain-on-snow events, *Geophys Res Lett*, 42, 7115–  
781 7122, <https://doi.org/10.1002/2015GL065320>, 2015.

782 Collados-Lara, A. J., Pulido-Velazquez, D., Pardo-Igúzquiza, E., and Alonso-González, E.: Estimation of the  
783 spatio-temporal dynamic of snow water equivalent at mountain range scale under data scarcity, *Science of the*  
784 *Total Environment*, 741, <https://doi.org/10.1016/j.scitotenv.2020.140485>, 2020.

785 Conway, H. and Raymond, C. F.: Snow stability during rain, *Journal of Glaciology*, 39, 635–642,  
786 <https://doi.org/10.3189/s0022143000016531>, 1993.

787 Corripio, J. G. and López-Moreno, J. I.: Analysis and predictability of the hydrological response of mountain  
788 catchments to heavy rain on snow events: A case study in the Spanish Pyrenees, *Hydrology*, 4,  
789 <https://doi.org/10.3390/hydrology4020020>, 2017.

790

791 Deschamps-Berger, C., Cluzet, B., Dumont, M., Lafaysse, M., Berthier, E., Fanise, P., and Gascoin, S.:  
792 Improving the Spatial Distribution of Snow Cover Simulations by Assimilation of Satellite Stereoscopic  
793 Imagery, *Water Resour. Res.*, 58, e2021WR030271, <https://doi.org/10.1029/2021WR030271>, 2022.

794

795 Del Barrio, G., Creus, J., and Puigdefàbregas, J.: Thermal Seasonality of the High Mountain Belts of the  
796 Pyrenees, *Mt. Res. Dev.*, 10, 227–233, 1990.

797 Durand, Y., Giraud, G., Brun, E., Mérindol, L., and Martin, E.: A computer-based system simulating snowpack  
798 structures as a tool for regional avalanche forecasting, *Journal of Glaciology*, 45, 469–484,  
799 <https://doi.org/10.3189/s0022143000001337>, 1999.

800 Durand, Y., Laternser, M., Giraud, G., Etchevers, P., Lesaffre, B., and Mérindol, L.: Reanalysis of 44 yr of  
801 climate in the French Alps (1958-2002): Methodology, model validation, climatology, and trends for air  
802 temperature and precipitation, *J Appl Meteorol Climatol*, 48, 429–449,  
803 <https://doi.org/10.1175/2008JAMC1808.1>, 2009.

804 Essery, R.: A factorial snowpack model (FSM 1.0), *Geosci Model Dev*, 8, 3867–3876,  
805 <https://doi.org/10.5194/gmd-8-3867-2015>, 2015.

806

807 Essery, R., Kim, H., Wang, L., Bartlett, P., Boone, A., Brutel-Vuilmet, C., Burke, E., Cuntz, M., Decharme,  
808 B., Dutra, E., Fang, X., Gusev, Y., Hagemann, S., Haverd, V., Kontu, A., Krinner, G., Lafaysse, M., Lejeune,  
809 Y., Marke, T., Marks, D., Marty, C., Menard, C. B., Nasonova, O., Nitta, T., Pomeroy, J., Schädler, G.,  
810 Semenov, V., Smirnova, T., Swenson, S., Turkov, D., Wever, N., and Yuan, H.: Snow cover duration trends  
811 observed at sites and predicted by multiple models, *Cryosphere*, 14, 4687–4698, [https://doi.org/10.5194/tc-](https://doi.org/10.5194/tc-14-4687-2020)  
812 [14-4687-2020](https://doi.org/10.5194/tc-14-4687-2020), 2020.

813 Freudiger, D., Kohn, I., Stahl, K., and Weiler, M.: Large-scale analysis of changing frequencies of rain-on-  
814 snow events with flood-generation potential, *Hydrol Earth Syst Sci*, 18, 2695–2709,

815 <https://doi.org/10.5194/hess-18-2695-2014>, 2014.

816 García-Ruiz, J. M., López-Moreno, J. I., Vicente-Serrano, S. M., Lasanta-Martínez, T. and Beguería, S.  
817 Mediterranean water resources in a global change scenario, *Earth Sci. Rev.*, 105(3–4), 121–139,  
818 <https://doi.org/10.1016/j.earscirev.2011.01.006>, 2011.

819 Garvelmann, J., Pohl, S., and Weiler, M.: Variability of observed energy fluxes during rain-on-snow and clear  
820 sky snowmelt in a midlatitude mountain environment, *J Hydrometeorol*, 15, 1220–1237,  
821 <https://doi.org/10.1175/JHM-D-13-0187.1>, 2014.

822 Günther, D., Marke, T., Essery, R., and Strasser, U.: Uncertainties in Snowpack Simulations—Assessing the  
823 Impact of Model Structure, Parameter Choice, and Forcing Data Error on Point-Scale Energy Balance Snow  
824 Model Performance, *Water Resour Res*, 55, 2779–2800, <https://doi.org/10.1029/2018WR023403>, 2019.

825 Hansen, B.B., Isaksen, K., Benestad, R.E., et al.. Warmer and wetter winters: characteristics and implications  
826 of an extreme weather event in the High Arctic. *Environ. Res. Lett.* 9, 114021.

827 Harder, P. and Pomeroy, J.: Hydrological model uncertainty due to precipitation-phase partitioning methods,  
828 *Hydrological Processes*, 28, 4311–4327. <https://doi.org/10.1002/hyp.9799>, 2014.

829 Hock, R.,—Rasul, G.,—Adler, C.,—Cáceres, B.,—Gruber, S.,—Hirabayashi, Y.,—Jackson, M.,—Käab, A.,  
830 Kang, S.,—Kutuzov, S.,—Milner, A.I.,—Molau, U.,—Morin, S.,—Orlove, B.,—and Steltzer, H.: High  
831 Mountain Areas, in: *IPCC Special Report on the Ocean and Cryosphere in a Changing Climate*, edited  
832 by: Pörtner, H.-O.,—Roberts, D. C.,—Masson-Delmotte, V.,—Zhai, P.,—Tignor, M.,—Poloczanska, E.,  
833 Mintenbeck, K.,—Alegria, A.,—Nicolai, M.,—Okem, A.,—Petzold, J.,—Rama, B.,—and Weyer, N.M. Cambridge  
834 University Press, Cambridge, UK and New York, —NY, —USA, —pp. 131–202.  
835 <https://doi.org/10.1017/9781009157964.004>, 2019.

836 Immerzeel, W. W., Lutz, A. F., Andrade, M., Bahl, A., Biemans, H., Bolch, T., Hyde, S., Brumby, S., Davies,  
837 B. J., Elmore, A. C., Emmer, A., Feng, M., Fernández, A., Haritashya, U., Kargel, J. S., Koppes, M.,  
838 Kraaijenbrink, P. D. A., Kulkarni, A. v., Mayewski, P. A., Nepal, S., Pacheco, P., Painter, T. H., Pellicciotti, F.,  
839 Rajaram, H., Rupper, S., Sinisalo, A., Shrestha, A. B., Viroli, D., Wada, Y., Xiao, C., Yao, T., and Baillie, J.  
840 E. M.: Importance and vulnerability of the world's water towers, *Nature*, 577, 364–369,  
841 <https://doi.org/10.1038/s41586-019-1822-y>, 2020.

842 Jennings, K. S., Winchell, T. S., Livneh, B., and Molotch, N. P.: Spatial variation of the rain-snow temperature  
843 threshold across the Northern Hemisphere, *Nat Commun*, 9, <https://doi.org/10.1038/s41467-018-03629-7>,  
844 2018.

845 il Jeong, D. and Sushama, L.: Rain-on-snow events over North America based on two Canadian regional  
846 climate models, *Clim Dyn*, 50, 303–316, <https://doi.org/10.1007/s00382-017-3609-x>, 2018.

847 Kohler, J. and Aanes, R.: Effect of winter snow and ground-icing on a Svalbard reindeer population: Results  
848 of a simple snowpack model, in: *Arctic, Antarctic, and Alpine Research*, 333–341,  
849 [https://doi.org/10.1657/1523-0430\(2004\)036\[0333:EOWSAG\]2.0.CO;2](https://doi.org/10.1657/1523-0430(2004)036[0333:EOWSAG]2.0.CO;2), 2004.

850 Krinner, G., Derksen, C., Essery, R., Flanner, M., Hagemann, S., Clark, M., Hall, A., Rott, H., Brutel-  
851 Vuilmet, C., Kim, H., Ménard, C. B., Mudryk, L., Thackeray, C., Wang, L., Arduini, G., Balsamo, G.,  
852 Bartlett, P., Boike, J., Boone, A., Chérut, F., Colin, J., Cuntz, M., Dai, Y., Decharme, B., Derry, J.,  
853 Ducharme, A., Dutra, E., Fang, X., Fierz, C., Ghattas, J., Gusev, Y., Haverd, V., Kontu, A., Lafaysse, M.,  
854 Law, R., Lawrence, D., Li, W., Marke, T., Marks, D., Ménégoz, M., Nasonova, O., Nitta, T., Niwano, M.,

855 Pomeroy, J., Raleigh, M. S., Schaedler, G., Semenov, V., Smirnova, T. G., Stacke, T., Strasser, U.,  
856 Svenson, S., Turkov, D., Wang, T., Wever, N., Yuan, H., Zhou, W., and Zhu, D.: ESM-SnowMIP: assessing  
857 snow models and quantifying snow-related climate feedbacks, *Geosci. Model Dev.*, 11, 5027–5049,  
858 <https://doi.org/10.5194/gmd-11-5027-2018>, 2018.

859 Lemus-Canovas, M., Lopez-Bustins, J. A., Trapero, L., and Martin-Vide, J.: Combining circulation weather  
860 types and daily precipitation modelling to derive climatic precipitation regions in the Pyrenees, *Atmos Res*,  
861 220, 181–193, <https://doi.org/10.1016/j.atmosres.2019.01.018>, 2019.

862 Lemus-Canovas, M., Lopez-Bustins, J. A., Martín-Vide, J., Halifa-Marin, A., Insua-Costa, D., Martínez-  
863 Artigas, J., Trapero, L., Serrano-Notivoli, R., and Cuadrat, J. M.: Characterisation of extreme precipitation  
864 events in the Pyrenees: From the local to the synoptic scale, *Atmosphere (Basel)*, 12,  
865 <https://doi.org/10.3390/atmos12060665>, 2021.

866 Li, D., Lettenmaier, D. P., Margulis, S. A., and Andreadis, K.: The Role of Rain-on-Snow in Flooding Over  
867 the Conterminous United States, *Water Resour Res*, 55, 8492–8513, <https://doi.org/10.1029/2019WR024950>,  
868 2019.

869 Llasat, M. C., Marcos, R., Llasat-Botija, M., Gilabert, J., Turco, M., and Quintana-Seguí, P.: Flash flood  
870 evolution in North-Western Mediterranean, *Atmos Res*, 149, 230–243,  
871 <https://doi.org/10.1016/j.atmosres.2014.05.024>, 2014.

872 López-Moreno, J. I.: Recent variations of snowpack depth in the central Spanish Pyrenees, *Arct Antarct Alp*  
873 *Res*, 37, 253–260, [https://doi.org/10.1657/1523-0430\(2005\)037\[0253:RVOSDI\]2.0.CO;2](https://doi.org/10.1657/1523-0430(2005)037[0253:RVOSDI]2.0.CO;2), 2005.

874 López-Moreno, J. I., Goyette, S., and Beniston, M.: Climate change prediction over complex areas: spatial  
875 variability of uncertainties and predictions over the Pyrenees from a set of regional climate models.  
876 *International Journal of Climatology*, 28, 1535–1550. <https://doi.org/10.1002/joc.1645>, 2008.

877 López-Moreno, J. I., Pomeroy, J. W., Revuelto, J., and Vicente-Serrano, S. M.: Response of snow processes to  
878 climate change: Spatial variability in a small basin in the Spanish Pyrenees, *Hydrol Process*, 27, 2637–2650,  
879 <https://doi.org/10.1002/hyp.9408>, 2013.

880 López-Moreno, J. I., Pomeroy, J. W., Morán-Tejeda, E., Revuelto, J., Navarro-Serrano, F. M., Vidaller, I., and  
881 Alonso-González, E.: Changes in the frequency of global high mountain rain-on-snow events due to climate  
882 warming, *Environmental Research Letters*, 16, <https://doi.org/10.1088/1748-9326/ac0dde>, 2021.

883 López-Moreno, J. I., Soubeyroux, J. M., Gascoin, S., Alonso-González, E., Durán-Gómez, N., Lafaysse, M.,  
884 Vernay, M., Carmagnola, C. and Morin, S. Long-term trends (1958–2017) in snow cover duration and depth  
885 in the Pyrenees. *International Journal of Climatology*, 40, 1–15. <https://doi.org/10.1002/joc.6571>, 2020.

886 López-Moreno, J. I., and Vicente-Serrano, S. M.: Atmospheric circulation influence on the interannual  
887 variability of snowpack in the Spanish Pyrenees during the second half of the twentieth century, *Nord. Hydrol.*,  
888 38 (1), 38–44, <https://doi.org/10.2166/nh.2007.030>, 2007.

889 López-Moreno, J. I., and Latron, J., 2008. Spatial heterogeneity in snow water equivalent induced by forest  
890 canopy in a mixed beech-fir stand in the Pyrenees. *Ann. Glaciol.* 49 (1), 83–90,  
891 <https://doi.org/10.3189/172756408787814951>, 2008.

892 Loukas, A., Vasiliades, L., and Dalezios, N. R.: Potential climate change impacts on flood producing  
893 mechanisms in southern British Columbia, Canada using the CGCMA1 simulation results, *J. Hydrol.*, 259,

894 163–188, [https://doi.org/10.1016/S0022-1694\(01\)00580-7](https://doi.org/10.1016/S0022-1694(01)00580-7), 2002

895 Lundquist, J. D., Dickerson-Lange, S. E., Lutz, J. A., and Cristea, N. C.: Lower forest density enhances snow  
 896 retention in regions with warmer winters: A global framework developed from plot-scale observations and  
 897 modeling, *Water Resour Res*, 49, 6356–6370, <https://doi.org/10.1002/wrcr.20504>, 2013.

898 Lynn, E., Cuthbertson, A., He, M., Vasquez, J. P., Anderson, M. L., Coombe, P., Abatzoglou, J. T., and Hatchett,  
 899 B. J.: Technical note: Precipitation-phase partitioning at landscape scales to regional scales, *Hydrol Earth Syst*  
 900 *Sci*, 24, 5317–5328, <https://doi.org/10.5194/hess-24-5317-2020>, 2020.

901 Matiu, M., Crespi, A., Bertoldi, G., Carmagnola, C.M., Marty, C., Morin, S., Schöner, W., Cat Berro, D.,  
 902 Chiogna, G., De Gregorio, L., Kotlarski, S., Majone, B., Resch, G., Terzago, S., Valt, M., Beozzo, W.,  
 903 Cianfarra, P., Gouttevin, I., Marcolini, G., Notarnicola, C., Petitta, M., Scherrer, S.C., Strasser, U., Winkler,  
 904 M., Zebisch, M., Cicogna, A., Cremonini, R., Debernardi, A., Faletto, M., Gaddo, M., Giovannini, L., Mercalli,  
 905 L., Soubeyroux, J.-M., Susnik, A., Trenti, A., Urbani, S., Weilguni, V. Observed snow depth trends in the  
 906 European Alps 1971 to 2019. *Cryosphere*, 1–50. <https://doi.org/10.5194/tc-2020-289>, 2020.

907 Marks, D., Link, T., Winstral, A., and Garen, D.: Simulating snowmelt processes during rain-on-snow over a  
 908 semi-arid mountain basin, 1992.

909

910 Martin, E., Brun, E., and Durand, Y.: Sensitivity of the French Alps snow cover to the variation of climatic  
 911 variables, *Annales Geophysicae*, 12, 469–477, 1994.

912 Marty, C., Schlögl, S., Bavay, M., and Lehning, M.: How much can we save? Impact of different emission  
 913 scenarios on future snow cover in the Alps, *Cryosphere*, 11, 517–529, <https://doi.org/10.5194/tc-11-517-2017>,  
 914 2017.

915 Mazurkiewicz, A. B., Callery, D. G., and McDonnell, J. J.: Assessing the controls of the snow energy balance  
 916 and water available for runoff in a rain-on-snow environment, *J Hydrol (Amst)*, 354, 1–14,  
 917 <https://doi.org/10.1016/j.jhydrol.2007.12.027>, 2008.

918 Mazzotti, G., Essery, R., Webster, C., Malle, J., and Jonas, T.: Process-Level Evaluation of a Hyper-Resolution  
 919 Forest Snow Model Using Distributed Multisensor Observations, *Water Resour Res*, 56,  
 920 <https://doi.org/10.1029/2020WR027572>, 2020.

921 McCabe, G. J., Clark, M. P., and Hay, L. E.: Rain-on-snow events in the Western ~~United States~~ United States,  
 922 <https://doi.org/10.1175/BAMS-88-3-319>, 2007.

923 Mooney, P. A. and Li, L.: Near future changes to rain-on-snow events in Norway, *Environmental Research*  
 924 *Letters*, 16, <https://doi.org/10.1088/1748-9326/abfdeb>, 2021.

925 Morán-Tejeda, E., López-Moreno, J. I., Stoffel, M., and Beniston, M.: Rain-on-snow events in Switzerland:  
 926 Recent observations and projections for the 21st century, *Clim Res*, 71, 111–125,  
 927 <https://doi.org/10.3354/cr01435>, 2016.

928 Morán-Tejeda, E., Fassnacht, S. R., Lorenzo-Lacruz, J., López-Moreno, J. I., García, C., Alonso-González, E.,  
 929 and Collados-Lara, A. J.: Hydro-meteorological characterization of major floods in Spanish mountain rivers,  
 930 *Water (Switzerland)*, 11, <https://doi.org/10.3390/W11122641>, 2019.

931 Morin, S., Horton, S., Techel, F., Bavay, M., Coléou, C., Fierz, C., Gobiet, A., Hagenmuller, P., Lafaysse, M.,

932 Ližar, M., Mitterer, C., Monti, F., Müller, K., Olefs, M., Snook, J. S., van Herwijnen, A., and Vionnet, V.:  
 933 Application of physical snowpack models in support of operational avalanche hazard forecasting: A status  
 934 report on current implementations and prospects for the future,  
 935 <https://doi.org/10.1016/j.coldregions.2019.102910>, 2020.

936 Musselman, K. N., Clark, M. P., Liu, C., Ikeda, K., and Rasmussen, R.: Slower snowmelt in a warmer world,  
 937 *Nat Clim Chang*, 7, 214–219, <https://doi.org/10.1038/nclimate3225>, 2017a.

938 Musselman, K. N., Keitholotch, N. P., Mar, N., and Mgulis, S. A.: Snowmelt response to simulated warming  
 939 across a large elevation gradient, southern sierra Nevada, California, *Cryosphere*, 11, 2847–2866,  
 940 <https://doi.org/10.5194/tc-11-2847-2017>, 2017b.

941 Musselman, K. N., Lehner, F., Ikeda, K., Clark, M. P., Prein, A. F., Liu, C., Barlage, M., and Rasmussen, R.:  
 942 Projected increases and shifts in rain-on-snow flood risk over ~~western~~Western North America,  
 943 <https://doi.org/10.1038/s41558-018-0236-4>, 2018.

944 Navarro-Serrano, F. and López-Moreno, J. I.: Análisis espacio-temporal de los eventos de nevadas en el pirineo  
 945 Español y su relación con la circulación atmosférica, *Cuadernos de Investigacion Geografica*, 43, 233–254,  
 946 <https://doi.org/10.18172/cig.3042>, 2017.

947 Ohba, M. and Kawase, H.: Rain-on-Snow events in Japan as projected by a large ensemble of regional climate  
 948 simulations, *Clim Dyn*, 55, 2785–2800, <https://doi.org/10.1007/s00382-020-05419-8>, 2020.

949  
 950 OPCC-CTP. Climate change in the Pyrenees: Impacts, vulnerabilities and adaptation bases of knowledge for  
 951 the future climate change adaptation strategy in the Pyrenees. 2018. 147. Jaca, Spain.  
 952 <https://www.opccctp.org/sites/default/files/editor/opcc-informe-en-paginas.pdf>. (last acces December 25,  
 953 2022)

954 Pall, P., Tallaksen, L. M., and Stordal, F.: A Climatology of Rain-on-Snow Events for Norway,  
 955 <https://doi.org/10.1175/JCLI-D-18>, 2019.

956 Pepin, N. C., Arnone, E., Gobiet, A., Haslinger, K., Kotlarski, S., Notarnicola, C., Palazzi, E., Seibert, P.,  
 957 Serafin, S., Schöner, W., Terzago, S., Thornton, J. M., Vuille, M., and Adler, C.: Climate Changes and Their  
 958 Elevational Patterns in the Mountains of the World, <https://doi.org/10.1029/2020RG000730>, 2022.

959 Peña-Angulo, D., Vicente-Serrano, S., Domínguez-Castro, F., Murphy, C., Reig, F., Trambly, Y., Trigo, R.,  
 960 Luna, M. Y., Turco, M., Noguera, I., Aznarez-Balta, M., Garcia-Herrera, R., Tomas-Burguera, M. and Kenawy,  
 961 A. Long-term precipitation in South~~western~~Western Europe reveals no clear trend attributable to anthropogenic  
 962 forcing. *Environmental Research Letters*, 15, 094070 <https://doi.org/10.1088/1748-9326/ab9c4f>, 2020.

963 Pons, M., López-Moreno, J., Rosas-Casals, M., and Jover, E.: The vulnerability of Pyrenean ski resorts to  
 964 climate-induced changes in the snowpack, *Clim.Change*, 131, 591–605, [https://doi.org/10.1007/s10584-015-](https://doi.org/10.1007/s10584-015-1400-8)  
 965 [1400-8](https://doi.org/10.1007/s10584-015-1400-8), 2015.

966 Pomeroy, J. W., Fang, X., and Rasouli, K.: Sensitivity of snow processes to warming in the Canadian Rockies,  
 967 2015.

968 Pomeroy, J. W., Fang, X., and Marks, D. G.: The cold rain-on-snow event of June 2013 in the Canadian Rockies  
 969 — characteristics and diagnosis, *Hydrol Process*, 30, 2899–2914, <https://doi.org/10.1002/hyp.10905>, 2016.

970 Rasouli, K., Pomeroy, J. W., and Whitfield, P. H.: Hydrological responses of headwater basins to monthly

971 perturbed climate in the North American Cordillera, *J Hydrometeorol*, 20, 863–882,  
972 <https://doi.org/10.1175/JHM-D-18-0166.1>, 2019.

973 Rennert, K. J., Roe, G., Putkonen, J., and Bitz, C. M.: Soil thermal and ecological impacts of rain on snow  
974 events in the circumpolar arctic, *J Clim*, 22, 2302–2315, <https://doi.org/10.1175/2008JCLI2117.1>, 2009.

975 Réveillet, M., Dumont, M., Gascoin, S., Lafaysse, M., Nabat, P., Ribes, A., Nheili, R., Tuzet, F., Ménégos, M.,  
976 Morin, S., Picard, G., and Ginoux, P.: Black carbon and dust alter the response of mountain snow cover under  
977 climate change, *Nat Commun*, 13, <https://doi.org/10.1038/s41467-022-32501-y>, 2022.

978 Revuelto, J., Lecourt, G., Lafaysse, M., Zin, I., Charrois, L., Vionnet, V., Dumont, M., Rabatel, A., Six, D.,  
979 Condom, T., Morin, S., Viani, A., and Sirguey, P.: Multi-criteria evaluation of snowpack simulations in  
980 complex alpine terrain using satellite and in situ observations, *Remote Sens (Basel)*, 10,  
981 <https://doi.org/10.3390/rs10081171>, 2018.

982 Roe, G. H. and Baker, M. B.: *Microphysical and Geometrical Controls on the Pattern of Orographic*  
983 *Precipitation*, 2006.

984 Sanmiguel-Valladolid, A., McPhee, J., Esmeralda Ojeda Carreño, P., Morán-Tejeda, E., Julio Camarero, J., and  
985 López-Moreno, J. I.: Sensitivity of forest–snow interactions to climate forcing: Local variability in a Pyrenean  
986 valley, *J Hydrol (Amst)*, 605, <https://doi.org/10.1016/j.jhydrol.2021.127311>, 2022.

987 Schirmer, M., Winstral, A., Jonas, T., Burlando, P., and Peleg, N.: Natural climate variability is an important  
988 aspect of future projections of snow water resources and rain-on-snow events, *Cryosphere*, 16, 3469–3488,  
989 <https://doi.org/10.5194/tc-16-3469-2022>, 2022.

990 Schöner, W., Koch, R., Matulla, C., Marty, C., and Tilg, A. M.: Spatio-temporal patterns of snow depth within  
991 the Swiss-Austrian Alps for the past half century (1961 to 2012) and linkages to climate change, *International*  
992 *Journal of Climatology*, 39, 1589–1603, <https://doi.org/10.1002/joc.5902>, 2019.

993 Serrano-Notivol, R., Buisan, S.T., Abad-Pérez, L.M., Sierra-Álvarez, E., Rodríguez-Ballesteros, C., López-  
994 Moreno, J.I. and Cuadrat, J.M. Tendencias recientes en precipitación, temperatura y nieve de alta montaña en  
995 los Pirineos (Refugio de Góriz, Huesca). In: *El clima: aire, agua, tierra y fuego*. Madrid, Spain: Asociación  
996 Española de Climatología y Ministerio para la Transición Ecológica – Agencia Estatal de Meteorología, pp.  
997 267, 1060–280, 2018.

998 Serrano-Notivol, R., Mora, D., Ollero, A., Sánchez-Fabre, M., Sanz, P., and Saz, M.: Floodplain occupation  
999 and flooding in the central Pyrenees, *Cuadernos de Investigacion Geografica*, 43, 309–328,  
1000 <https://doi.org/10.18172/cig.3057>, 2017.

1001 Shanley, J. B. and Chalmers, A.: The effect of frozen soil on snowmelt runoff at Sleepers River, Vermont 1999.

1002 Singh, P., Spitzbart, G., Hübl, H., and Weinmeister, H. W.: Hydrological response of snowpack under rain-on-  
1003 snow events: a field study, *Journal of Hydrology*, 1–20 pp., 1997.

1004 Spandre, P., François, H., Verfaillie, D., Lafaysse, M., Déqué, M., Eckert, N., George, E., and Morin, S.:  
1005 Climate controls on snow reliability in French Alps ski resorts, *Sci Rep*, 9, <https://doi.org/10.1038/s41598-1006-019-44068-8>, 2019.

1007 Stewart, I. T.: Changes in snowpack and snowmelt runoff for key mountain regions,  
1008 <https://doi.org/10.1002/hyp.7128>, 2009.

1009 Surfleet, C. G. and Tullos, D.: Variability in effect of climate change on rain-on-snow peak flow events in a



temperate climate, *J Hydrol (Amst)*, 479, 24–34, <https://doi.org/10.1016/j.jhydrol.2012.11.021>, 2013.

Szczypta, C., Gascoin, S., Houet, T., Hagolle, O., Dejoux, J.-F., Vigneau, C., and Fanise, P.: Impact of climate and land cover changes on snow cover in a small Pyrenean catchment, *J. Hydrol.*, 521, 84–99, doi:10.1016/j.jhydrol.2014.11.060, 2015.

Verfaillie, D., Lafaysse, M., Déqué, M., Eckert, N., Lejeune, Y., and Morin, S.: Multi-component ensembles of future meteorological and natural snow conditions for 1500 m altitude in the Chartreuse mountain range, Northern French Alps, *Cryosphere*, 12, 1249–1271, <https://doi.org/10.5194/tc-12-1249-2018>, 2018.

Vernay, M., Lafaysse, M., Monteiro, D., Hagenmuller, P., Nheili, R., Samacoïts, R., Verfaillie, D., and Morin, S.: The S2M meteorological and snow cover reanalysis over the French mountainous areas: description and evaluation (1958–2021), *Earth Syst Sci Data*, 14, 1707–1733, <https://doi.org/10.5194/essd-14-1707-2022>, 2022.

Vicente-Serrano, S.M., Rodríguez-Camino, E., Domínguez-Castro, F., El Kenawy, A., Azorín-Molina, C. An updated review on recent trends in observational surface atmospheric variables and their extremes over Spain. *Cuadernos de Investigación Geográfica (Geographical Research Letters)* 43 (1), 209–232. <https://doi.org/10.18172/cig.3134>, 2017.

Vidaller, I., Revuelto, J., Izagirre, E., Rojas-Heredia, F., Alonso-González, E., Gascoin, S., René, P., Berthier, E., Rico, I., Moreno, A., Serrano, E., Serreta, A., López-Moreno, J.I. Toward an ice-free mountain range: Demise of Pyrenean glaciers during 2011–2020. *J. Geophys. Res. Lett.* 48, e2021GL094339 <https://doi.org/10.1029/2021GL094339>, 2021.

Viviroli, D., Archer, D. R., Buytaert, W., Fowler, H. J., Greenwood, G. B., Hamlet, A. F., Huang, Y., Koboltschnig, G., Litaor, M. I., López-Moreno, J. I., Lorentz, S., Schädler, B., Schreier, H., Schwaiger, K., Vuille, M., and Woods, R.: Climate change and mountain water resources: Overview and recommendations for research, management and policy, *Hydrol Earth Syst Sci*, 15, 471–504, <https://doi.org/10.5194/hess-15-471-2011>, 2011.

Westermann, S., Boike, J., Langer, M., Schuler, T. V., and Etzelmüller, B.: Modeling the impact of wintertime rain events on the thermal regime of permafrost, *Cryosphere*, 5, 945–959, <https://doi.org/10.5194/tc-5-945-2011>, 2011.

Wipf, S. and Rixen, C.: A review of snow manipulation experiments in Arctic and alpine tundra ecosystems, <https://doi.org/10.1111/j.1751-8369.2010.00153.x>, 2010.

Wu, X., Che, T., Li, X., Wang, N., and Yang, X.: Slower Snowmelt in Spring Along With Climate Warming Across the Northern Hemisphere, *Geophys Res Lett*, 45, 12,331–12,339, <https://doi.org/10.1029/2018GL079511>, 2018.

Würzer, S., Jonas, T., Wever, N., and Lehning, M.: Influence of initial snowpack properties on runoff formation during rain-on-snow events, *J Hydrometeorol*, 17, 1801–1815, <https://doi.org/10.1175/JHM-D-15-0181.1>, 2016.